Scribble Deficiency Promotes Pancreatic Ductal Adenocarcinoma Development and Metastasis.

Camino Bermejo-Rodriguez[1], Joaquín Araos Henríquez[2, §], Giuseppina Caligiuri[3, §], Sara Pinto Teles[2], Youngkyu Park[3], Anthony Evans[1], Lawrence N. Barrera[1], Albrecht Neesse[4], Robert Grützmann[5], Daniela Aust[6, 7], Petra Rümmele[8], Thomas Knösel[9], Masako Narita[2], Masashi Narita[2], Fiona Campbell[10], Daniel Öhlund[11], Christian Pilarsky[12], Lukas E. Dow[13], Patrick O. Humbert[14], Giulia Biffi[2], David A. Tuveson[3, *], Pedro A. Perez-Mancera[1, *].

[1] Department of Molecular and Clinical Cancer Medicine, University of Liverpool, L69 3GE Liverpool, UK.

[2] Cancer Research UK Cambridge Institute, University of Cambridge, Cambridge, UK.

[3] Cold Spring Harbor Laboratory, Cold Spring Harbor, NY 11724 USA; and Lustgarten Foundation Pancreatic Cancer Research Laboratory, Cold Spring Harbor, NY 11724 USA.

[4] Department of Gastroenterology, Gastrointestinal Oncology and Endocrinology, University Medical Centre Goettingen, Goettingen, Germany.

[5] Department of Surgery, Universitätsklinikum Erlangen, Erlangen, Germany.

[6] Institute for Pathology, University Hospital Carl Gustav Carus, Dresden, Germany.

[7] Biobank Dresden, National Center for Tumor Diseases Dresden (NCT/UCC), Dresden, Germany.

[8] Institute of Pathology, Universitätsklinikum Erlangen, Erlangen, Germany.

[9] Institute of Pathology, Ludwig-Maximilians-Universität (LMU) Munich, Munich, Germany.

[10] Department of Pathology, Royal Liverpool University Hospital, Liverpool, UK.

[11] Department of Radiation Sciences, Umeå University, Umeå, Sweden; and Wallenberg Centre for Molecular Medicine, Umeå University, Umeå, Sweden.

[12] Department of Surgery, Uniklinikum Erlangen, Friedrich-Alexander Universität Erlangen-Nürnberg (FAU), Erlangen, Germany.

[13] Department of Biochemistry, Weill Cornell Medicine, New York, New York, USA.

[14] Department of Biochemistry & Chemistry, La Trobe Institute for Molecular Science, La Trobe University, Melbourne, Victoria, Australia.

[§]These authors contributed equally to this work.

[*]Co-corresponding authors: *dtuveson@cshl.edu*; *pedro.perez-mancera@liverpool.ac.uk*.

Running Title: Scribble Deficiency Promotes PDAC Development.

Correspondence:
*Pedro A. Perez-Mancera
Department of Molecular and Clinical Cancer Medicine,
University of Liverpool, L69 3GE Liverpool, UK.
T: +44 (0) 151 795 8033
pedro.perez-mancera@liverpool.ac.uk

*David A. Tuveson
Cold Spring Harbor Laboratory
Cold Spring Harbor, NY 11724, USA.
T: +1 516-367-5246
dtuveson@cshl.edu

Conflict of Interest: The authors declare no potential conflicts of interest.

ABSTRACT

Perturbation of cell polarity is a hallmark of pancreatic ductal adenocarcinoma (PDAC) progression. Scribble (SCRIB) is a well characterized polarity regulator that has diverse roles in the pathogenesis of human neoplasms. To investigate the impact of SCRIB deficiency in PDAC development and progression, *Scrib* expression was genetically ablated in well-established mouse models of PDAC. *Scrib* loss in combination with *Kras*^{G12D} did not influence development of pancreatic intraepithelial neoplasms (PanIN) in mice. However, *Scrib* deletion cooperated with *Kras*^{G12D} and concomitant *Trp53* heterozygous deletion to promote invasive PDAC and metastatic dissemination, leading to reduced overall survival. Immunohistochemical and transcriptome analyses revealed that *Scrib*-null tumors display a pronounced reduction of collagen content and cancer associated fibroblasts (CAF) abundance. Mechanistically, interleukin 1α (IL1α) levels were reduced in *Scrib*-deficient tumors, and *Scrib* knockdown downregulated IL1α in mouse PDAC organoids (mPDOs), which impaired CAF activation. Furthermore, *Scrib* loss increased YAP activation in mPDOs and established PDAC cell lines, enhancing cell survival. Clinically, SCRIB expression was decreased in human PDAC, and SCRIB mislocalization was associated with poorer patient outcome. These results indicate that SCRIB deficiency enhances cancer cell survival and remodels the tumor microenvironment to accelerate PDAC development and progression, establishing the tumor suppressor function of SCRIB in advanced pancreatic cancer.

SIGNIFICANCE: SCRIB loss promotes invasive pancreatic cancer development via both cell-autonomous and non-cell-autonomous processes and is associated with poorer outcomes, denoting SCRIB as a tumor suppressor and potential biomarker for prediction of recurrence.

INTRODUCTION

Pancreatic ductal adenocarcinoma (PDAC) is an almost uniformly lethal disease with an innate propensity to develop distant metastasis (1,2). Histologically, PDAC typically arises from precursor lesions called pancreatic intraepithelial neoplasms (PanINs) (3). Activating mutations in *KRAS* are considered the earliest event in PDAC development, and induce the formation of low-grade PanIN lesions that progress through high-grade PanIN lesions and eventually invasive and lethal PDAC after the accumulation of additional genetic alterations, frequently including inactivation of *P16/CDKN2A*, *TP53* and *DPC4/SMAD4* (2-4). None of these mutations, however, explain the biological and clinical heterogeneity in pancreatic cancer (1,2). Therefore, a better understanding of the molecular basis underlying the aggressive biology of PDAC is crucial for developing novel therapeutic strategies to improve overall prognosis.

The correct establishment and maintenance of cell polarity is pivotal to preserve epithelial tissue architecture and homeostasis. Epithelial cell polarity is maintained by three apical-basal core polarity modules: the apical Par and Crumbs complexes, and the basolateral Scribble module (5,6). Cell polarity disruption is a main hallmark of PanIN-to-PDAC progression (3), and accumulating evidence has revealed that disruption of epithelial polarity dysregulates oncogenic and tumor suppressor signaling pathways leading to tumor progression and dissemination (6-9).

Scribble (SCRIB) is one of the best characterized polarity regulators (10,11). In *Drosophila melanogaster*, *Scrib* deficiency disrupts apical-basal polarity, induces tissue overgrowth and cooperates with oncogenic *Ras* in the development of epithelial tumors (12,13). The tumor suppressive properties of SCRIB have been validated in mouse models of cancer, including prostate, lung, skin and breast (14-18). Interestingly, oncogenic activities of SCRIB have also been exposed in mouse models of breast cancer and MYC-driven lymphoma (19,20), supporting a context dependent function for SCRIB. In human cancer, altered expression of SCRIB has been associated with the development of diverse neoplasias, including lung, prostate, breast and liver cancers (14,15,17,21,22).

Despite our understanding of SCRIB activity in tumor development, its relevance in PDAC remains largely unknown. To elucidate the role of SCRIB in pancreatic cancer development, we have undertaken a comprehensive approach to evaluate the impact of *Scrib* deficiency in the pathogenesis of PDAC. Using well-validated mouse models of $KRAS^{G12D}$-driven PDAC, mouse PDAC organoids, established mouse and human PDAC cell lines, RNA-sequencing (RNA-seq) analysis and evaluation of human PDAC specimens, we reveal that SCRIB functions as a tumor suppressor in an advanced stage of the disease. We show that the tumor suppressive activity of SCRIB is mediated via both cell-autonomous and non-cell-autonomous processes. Clinically, our data show that SCRIB mislocalization associates with poorer outcome, supporting the relevance of the altered expression of SCRIB in the development and progression of PDAC.

MATERIALS AND METHODS

Mouse strains

The *Kras*$^{LSL\text{-}G12D/+}$ (RRID:IMSR_JAX:008179) (23), *Trp53*$^{Flox/+}$ (24), *Scrib*$^{Flox/+}$ (14), *Pdx1*^{Cre} (25) and *Ptf1a/P48*$^{Cre/+}$ (26) strains were interbred to obtain *Kras*$^{LSL\text{-}G12D/+}$*; Pdx1*^{Cre} (KPdx1), *Kras*$^{LSL\text{-}G12D/+}$*; Pdx1*^{Cre}*; Scrib*$^{Flox/+}$ (KPdx1S$^{F/+}$), *Kras*$^{LSL\text{-}G12D/+}$*; Pdx1*^{Cre}*; Scrib*$^{Flox/Flox}$ (KPdx1S$^{F/F}$), *Kras*$^{LSL\text{-}G12D/+}$*; Ptf1a/P48*$^{Cre/+}$ (KP48), *Kras*$^{LSL\text{-}G12D/+}$*; Ptf1a/P48*$^{Cre/+}$*; Scrib*$^{Flox/+}$ (KP48S$^{F/+}$), *Kras*$^{LSL\text{-}G12D/+}$*; Ptf1a/P48*$^{Cre/+}$*; Scrib*$^{Flox/Flox}$ (KP48S$^{F/F}$), *Kras*$^{LSL\text{-}G12D/+}$*; Trp53*$^{Flox/+}$*; Pdx1*^{Cre} (KP$^{F/+}$C), *Kras*$^{LSL\text{-}G12D/+}$*; Trp53*$^{Flox/+}$*; Pdx1*^{Cre}*; Scrib*$^{Flox/+}$ (KP$^{F/+}$CS$^{F/+}$), *Kras*$^{LSL\text{-}G12D/+}$*; Trp53*$^{Flox/+}$*; Pdx1*^{Cre}*; Scrib*$^{Flox/Flox}$ (KP$^{F/+}$CS$^{F/F}$) and various littermate control animals on a mixed C57BL6/129Sv background. The animal cohorts included both males and females. Mice were housed, monitored daily, and tissues collected when exhibiting clinical deterioration. Mouse experiments were performed following ARRIVE guidelines and in compliance with the UK Home Office regulations (PPL802072 and PPL7008773).

Scrib^{Flox} recombination PCR

Genomic DNA was obtained from tails and pancreata of *Scrib*$^{Flox/Flox}$*, Pdx1*^{Cre}*; Scrib*$^{Flox/Flox}$ *and Ptf1a/P48*$^{Cre/+}$*; Scrib*$^{Flox/Flox}$ mice, and primers used to assess the recombination of the *Scrib*^{Flox} allele were: 3F (5′-GGAGATTGCAGACTTCAGTGG-3′), 6R (5′-GCTTCACCAGGAAAGACAGGG-3′) and 14R (5′-GACTCTGCACTCAGCCTCTTC-3′).

Cell lines and cell culture

Mouse pancreatic stellate cell lines (PSC4 and PSC5) derive from pancreata of wild-type mice and were previously generated and characterized (27). PSCs were cultured in DMEM (Gibco) supplemented with 3.97 mM L-Glutamine (Gibco), 5% FBS (Gibco) and 1% Penicillin/Streptomycin (Gibco). Mouse PDAC organoid (mPDO) lines (T91, T113 and T118) were previously generated from KP$^{F/F}$C mice (28) and cultured in complete organoid media (28,29). For conditioned media experiments, mPDOs were cultured in control media (DMEM supplemented with 3.97 mM L-Glutamine, 5% FBS and 1% Penicillin/Streptomycin) for 3 days. Then, PSCs were embedded within Matrigel (Corning) and cultured in conditioned media from PDAC organoids (with or without 20 pg/ml mouse IL1α (Bio-Techne)), or control media, for 4 days before RNA extraction. Mouse PDAC cell lines KP$^{F/+}$C#3 and KP$^{F/+}$C#9 were isolated from tumors arising in KP$^{F/+}$C mice using a protocol previously described (30), with small modifications. Briefly, a ~5mm^3 fragment of tumor was minced and enzymatically digested in collagenase solution at 37ºC for 30 minutes (3 mg/mL collagenase V (Sigma) in DMEM containing 5% FBS). Then, cells were spun (200g, 5 minutes) and resuspended in 0.05% Trypsin/EDTA (Gibco) for 5 minutes at 37ºC. Finally, cells were washed 3 times with DMEM containing 5% FBS and cultured in DMEM supplemented with 3.97 mM L-Glutamine, 10% FBS and 1% Penicillin/Streptomycin. Mouse embryonic fibroblasts (MEFs) were generated as previously described (31) and cultured in DMEM supplemented with 3.97 mM L-Glutamine, 10% FBS and 1% Penicillin/Streptomycin. The human cell line AsPC1 was obtained from ATCC (CRL-1682) and cultured in RPMI (Gibco) supplemented with 3.97 mM L-Glutamine, 10% FBS and 1% Penicillin/Streptomycin. Human cell lines PANC1, MiaPaCa2,

Hs766T, CFPAC1, PATU8902, RWP1, T3M4 and SUIT2 were obtained from Clare Hall Laboratories (CRUK) and cultured in DMEM supplemented with 3.97 mM L-Glutamine, 10% FBS and 1% Penicillin/Streptomycin. All cell lines tested negative for mycoplasma contamination using the e-Myco mycoplasma PCR detection kit (Chembio). Cell lines were authenticated by short-tandem repeat genetic profiling (STR).

Expression vectors

To knockdown the expression of mouse *Scrib*, short hairpin RNAs against *Scrib* (#613: 5'-CCGGAACGATATTCCTGAGATA -3' and #5523: 5'-AAAGACTCTATTTTGTGGTTTA-3') were cloned in the retroviral vector LENG (32). shScrib.5523 was used for functional analysis. To knockdown the expression of human *SCRIB*, a short hairpin RNA against *SCRIB* (#303: 5'-CGGAGAGCATCAAGTTCTGCAA -3') was cloned in the retroviral vector LEPG (32). A short hairpin RNA against *Renilla* (5'-CAGGAATTATAATGCTTATCTA-3') was used as control. The retroviral vectors MSCV-PURO-SCRIB^{WT} (RRID:Addgene_88886) and MSCV-PURO-SCRIB^{P305L} (RRID:Addgene_88887). The MCSV-PURO vector was used as control.

Retroviral infections

Phoenix cells (RRID:SCR_003163) were cultured in DMEM supplemented with 3.97 mM L-Glutamine, 10% FBS and 1% Penicillin/Streptomycin. Cells were transfected with retroviral vectors using a standard Calcium Phosphate protocol. For mPDOs, retroviruses were produced in ecotropic Phoenix packaging cells, concentrated with Retro-X Concentrator (Takara) and resuspended in organoid culture media supplemented with 10 mM Y-27632 (Sigma) in the presence of 8 µg/ml polybrene (Sigma). Infections were performed as previously described (29), and mPDOs selected with 800 µg/ml Neomycin (Takara). Mouse KP$^{F/+}$C cells were infected with retroviruses produced in ecotropic Phoenix packaging cells in the presence of 8 µg/ml polybrene (Sigma) and, 48 hours after infection, cells were selected with 800 µg/ml Neomycin (Takara). Experiments were performed using at least 2 pools of cells from independent infections. CFPAC1 and PATU8902 cells were infected with retroviruses produced in amphotropic Phoenix packaging cells in the presence of 8 µg/ml polybrene (Sigma) and, 48 hours after infection, cells were selected with 2 µg/ml Puromycin (Merck). Experiments were performed using at least 2 pools of cells from independent infections. Cells used in all experiments were below 5 (KP$^{F/+}$C, CFPAC1 and PATU8902) or 8 (mPDOs) passages after retroviral infections.

***In vitro* assays**

For anoikis assay, 6,000 cells were plated in poly-HEMA coated white 96 well-plates and cultured in 100 µl of DMEM-10% FBS. Apoptosis was assessed after 48 hours using the Caspase-Glo 3/7 Assay System (Promega). For cell viability assay of CFPAC1, 2,000 cells were plated in white 96 well-plates (5 replicates) and cultured in 100 µl of DMEM-10% FBS, or 80% HBSS/20% DMEM-10% FBS (2% FBS final concentration). Cell viability was assessed after 3 days with CellTiter-Glo Luminescent Cell Viability Assay (Promega). For cell viability assay of mPDOs, 1,500 single cells were plated in white 96 well-plates (5 replicates) in 100 µl of 10% Matrigel with organoid media (29) with or without the presence of 1 µM Verteporfin (Bio-techne). Cell viability was evaluated at days 1, 2 and 3 with CellTiter-Glo 3D

Luminescent Cell Viability Assay (Promega). For cell viability assay of PATU8902 cells, 2,000 cells were plated in white 96 well-plates (5 replicates) in 100 µl of DMEM-10% FBS with or without the presence of 4 µM Verteporfin (Bio-techne). Cell viability was evaluated at day 2 with CellTiter-Glo Luminescent Cell Viability Assay (Promega). For focus formation assay, $3x10^5$ CFPAC1 cells were plated in 6-well plates and grown for 10 days. Foci were visualized using phase-contrast microscopy and counted in 6 different X10 fields. When indicated, 4 µM Verteporfin was added 4 days after plating the cells, and foci were evaluated 6 days later using phase-contrast microscopy and counted in 5 different X10 fields. The number of replicates of each assay is indicated in the figure legends.

ELISA

mPDO cultures were grown for 4 days in DMEM-5% FBS. Media were collected and assayed using the Mouse IL-1 alpha/IL-1F1 Quantikine ELISA Kit (MLA00; R&D Systems) following the manufacturer's instructions.

Luciferase assay

CFPAC1 cells stably expressing $SCRIB^{WT}$ and $SCRIB^{P305L}$ were plated in 6-well plates at $5x10^5$ cells/well. The next day, cells were co-transfected with the YAP/TAZ-responsive reporter 8xGTIIC-luciferase (500 ng/well, RIDD:Addgene_34615) and pRL-SV40P (100 ng/well, RIDD:Addgene_27163) using Lipofectamine 3000 (Invitrogen) following the manufacturer's instructions. Forty-eight hours post-transfection, cells were lysed and Firefly/Renilla luciferase activity quantified by luminescence using the Dual-Luciferase Reporter Assay System (Promega) following the manufacturer's instructions.

Western blot analysis

mPDOs were washed three times in cold PBS (supplemented with PhosSTOP (Sigma) and Complete Mini, EDTA-free Protease Inhibitor Cocktail (Sigma)) and lysed with boiling lysis buffer (1% SDS; 10mM, pH 7.5 Tris; PhosSTOP and Complete Mini, EDTA-free Protease Inhibitor Cocktail). Human CFPAC1 and PATU8902 cells were washed three times in cold PBS and lysed with boiling lysis buffer (1% SDS; 10mM, pH 7.5 Tris; 50mM NaF; 1mM VO4). Lysates were boiled 5 minutes, passed through a 26-gauge needle, and centrifuged for 10 minutes at 14,000 rpm. Mouse PDAC tissues were disrupted and homogenized in boiling lysis buffer using the TissueLyser (Qiagen). Lysates were boiled 5 minutes, passed through a 26-gauge needle, and centrifuged for 10 minutes at 14,000 rpm. Equivalent amounts of protein were resolved in SDS-PAGE gels, transferred to Immobilon–P Transfer Membranes (Millipore), and incubated with the corresponding antibodies: anti-Scribble (Millipore Cat# MAB1820, RRID:AB_1587495, and Abcam Cat# ab154067), anti-p53 (BioVision Cat# 3036R-100, RRID:AB_992824), anti-YAP/TAZ (Cell Signaling Technology Cat# 8418, RRID:AB_10950494), anti-active (non-phosphorylated) YAP (Abcam Cat# ab205270, RRID:AB_2813833) and anti-β-ACTIN (Abcam Cat# ab6276, RRID:AB_2223210). Reactive bands were visualized with ECL Reagent (Amersham and Bio-Rad).

Immunofluorescence

Cells were grown on glass cover slips and fixed in cold methanol:acetone (1:1) (E-Cadherin) or 4% paraformaldehyde (SCRIB) for 15 minutes. Cells were then washed with PBSA (1% BSA in PBS), blocked for 45 minutes (PBSA/10% normal goat serum) and incubated with anti-SCRIB primary antibody (1:100, Santa Cruz Biotechnology Cat# sc-55543, RRID:AB_2238926) or anti-E-Cadherin primary antibody (1:200, BD Biosciences Cat# 610182, RRID:AB_397581). Alexa Fluor 488 secondary antibody (Life Technologies) was used to visualize SCRIB and E-Cadherin. Cells were mounted with Prolong Diamond Antifade Mountant with DAPI (Thermo Fisher Scientific). Images were acquired using a Zeiss Axio Observer Z1 microscope and analyzed using ImageJ (RRID:SCR_003070).

Gene expression by qPCR

Total RNA from mouse PDAC tissues was extracted using the RNeasy Plus Mini Kit (Qiagen) according to the manufacturer's instruction. Total RNA from PSCs and mPDOs were extracted using Trizol (Thermo Fisher Scientific). Then, RNA (1.5 µg) was reverse-transcribed into cDNA using the High-Capacity RNA-to-cDNA kit (Applied Biosystems). Gene expression was analyzed by quantitative PCR (qPCR) using PowerUp SYBR Green Master Mix (Applied Biosystems) and normalized to *Actb*. Relative quantification of gene expression was performed according to the $2^{-\Delta\Delta CT}$ method. A single peak in the melting curves confirmed primer specificity. The primer sequences and tumors used for qPCR analysis are provided in Supplementary Table 1.

Bulk RNA sequencing (RNA-seq) and data analysis

RNA concentration from PDAC tissues and mPDOs was measured using a Qubit and RNA quality was assessed on a 2100 Bioanalyzer (Agilent). mRNA library preparations were performed using 30 µL of 10 ng/mL (300 ng) per sample. Illumina libraries were then sequenced with an Illumina NovaSeq 6000. Estimated transcript counts were counted using Salmon (version 1.4.0) against the mouse reference genome GRCm38 (release 102) using default settings. Salmon estimated transcript counts were summarized to gene level using the tximport package in RStudio for use with DESeq2 (RRID:SCR_015687). Coding genes with fewer counts than 2^5 were filtered out before differential expression analysis (DEA). DEA was performed in R using DESeq package (V2) with default parameters. Genes with adjusted *P-value* < 0.05 were selected as significantly changed between conditions. Gene Set Enrichment Analysis (GSEA) of RNA-Seq Data (SeqGSEA (RRID:SCR_005724)) was performed using genes ranked by their *P-values* using the GSEA program (Broad Institute) on the Hallmark gene sets (h.all.v7.4) and the C2 canonical pathway collection (C2.all.v7.4) downloaded from the Molecular Signatures Database (MSigDB). Myofibroblastic CAF (myCAF) and inflammatory CAF (iCAF) signatures were derived from single-cell RNA-seq data of KPC tumours (33). All RNA-seq data are available at the Gene Expression Omnibus (GEO) (RRID:SCR_005012) under SuperSeries accession number GSE243939. This SuperSeries is composed of GSE193378 (mouse PDAC tumors) and GSE219196 (mouse PDAC organoids).

Mouse tissue immunohistochemistry and analysis

Formalin-fixed paraffin-embedded (FFPE) mouse tissues were cut into 5 µm tissue sections. Antigen retrieval was performed in 10 mM, pH 6.0 Citric Acid (E-Cadherin) or Tris-EDTA (α-SMA, PDPN and

IL1α). Endogenous peroxidases were quenched in 3% H_2O_2/PBS for 20 minutes. The primary antibodies used were E-Cadherin (1:200, BD Biosciences Cat# 610182, RRID:AB_397581), α-SMA (1:500, Abcam Cat# ab5694, RRID:AB_2223021), PDPN (1:150, BioLegend Cat# 127403, RRID:AB_1134221), anti-Cleaved Caspase-3 (1:300, Cell Signaling Technology Cat# 9664, RRID:AB_2070042), anti-Ki67 (1:400, Cell Signaling Technology Cat# 12202, RRID:AB_2620142) and mIL1α (1:50, Bio-techne Cat# AF-400-NA). Signal detection for E-Cadherin and α-SMA was accomplished with biotinylated secondary antibodies (Vector Laboratories) using the Elite Vectastain ABC kit and peroxidase substrate DAB kit (Vector Laboratories). Signal detection for PDPN, Cleaved Caspase-3, Ki67 and IL1α was accomplished using the Dako Envision kit (Dako). Slides were counterstained with hematoxylin. Images were acquired on an Aperio XT automated scanning system and Imagescope 10 software (Aperio) (RRID:SCR_014311). Automated quantification of α-SMA, PDPN and IL1α was performed using QuPath (https://qupath.github.io). Ki-67 and Cleaved Caspase-3 quantification was done manually by dividing the number of Ki67 positive neoplastic cells by the total number of counted neoplastic cells within gland-like structures. We quantified 10 different areas of the tumor that included a minimum of 1000 neoplastic cells. Sirius Red (Direct Red 80, Sigma) and Alcian Blue (8GX, Sigma) staining were performed according to the manufacturer's protocol. Sirius Red staining intensities were scored as absent (0), weak (1), moderate (2), strong (3) and very strong (4). The tumors used for immunohistochemical analysis are provided in Supplementary Table 1B.

Clinical patient sample immunohistochemistry and analysis

FFPE pancreatic tissue specimens (normal pancreas, PanIN and PDAC) were obtained after written informed consent from patients treated at Umeå University Hospital (Sweden). The study was conducted in accordance with the Declaration of Helsinki and was approved by the Regional Research Ethics Board of northern Sweden (Dnr. 09-175M/2009-1378-31 and 2019-00399). Immunohistochemistry was performed on 5 µm sections. Antigen retrieval was performed in Tris-EDTA. Endogenous peroxidases were quenched in 3% H_2O_2/PBS for 15 minutes. The primary antibody used was SCRIB (1:100, Santa Cruz Biotechnology Cat# sc-55543, RRID:AB_2238926). Signal detection was accomplished with biotinylated secondary antibodies (Vector Laboratories) using the Elite Vectastain ABC kit and peroxidase substrate DAB kit (Vector Laboratories). Slides were counterstained with hematoxylin.

Tissue microarrays were prepared from a second cohort of patient samples obtained after written informed consent in Dresden (Institute of Pathology, University Hospital Dresden), Regensburg (Institute of Pathology, University Hospital Regensburg) and Jena (Institute of Pathology, University Hospital Jena). The study was conducted in accordance with the Declaration of Helsinki and was approved by the Institutional Review Board of the Medical Faculty at the Technical University of Dresden (EK59032007). PDAC tumor samples were collected from 1993–2009, and most of the patients (65%) did not undergo adjuvant chemotherapy. Those that did undergo adjuvant therapy (35%) were chiefly treated with 5-FU or gemcitabine-based regimens, but in this subgroup there was no significant increase in patient survival. The median survival times of patients following surgery from each Institute were indistinguishable. Immunohistochemistry was performed on 5 µm sections that were prepared using silanized slides (Menzel Gläser, Braunschweig, Germany). Staining was performed with

the Benchmark System (Ventana, Illkirch, France), using mouse anti-SCRIB (1:50, Santa Cruz Biotechnology Cat# sc-55543, RRID:AB_2238926) and the protocol UltraView HRP, with the CC1 modified protocol as pre-treatment. Slides were counterstained with hematoxylin. Staining intensities were grouped as absent (0), weak (1), moderate (2) and strong (3).

Statistical analysis

Median survivals of mouse cohorts were assessed using the Kaplan-Meier method (log-rank test was used to statistically compare the curves). Statistical analyses of *in vitro* experiments were performed using Prism 7 (Graph Pad). Differences of quantified data were compared using t-test and Fisher's exact test for comparison between 2 groups, or one-way ANOVA with Bonferroni post-test for more than 2 groups. The immunohistochemistry scoring from human TMA samples and Kaplan-Meier survival curves were analyzed with SPSS18. Median survival difference was tested using the log-rank test. Asterisks denote *P-value* as follows: *$P < 0.05$, **$P < 0.01$, ***$P < 0.001$, ****$P < 0.0001$. $P < 0.05$ was considered statistically significant.

Data availability

RNA-seq data have been deposited in GEO under SuperSeries accession number GSE243939. This SuperSeries is composed of GSE193378 (mouse PDAC tumors) and GSE219196 (mouse PDAC organoids). All other raw data are available upon request from the corresponding authors.

RESULTS

***Scrib* ablation does not accelerate PanIN development in an oncogenic *Kras^{G12D}* background.**

Since germline inactivation of *Scrib* promotes embryonic lethality (14), we previously engineered a conditional *Scrib* floxed-allele (*Scrib^{Flox}*) and showed that *Scrib* deficiency cooperates with oncogenic *Kras^{G12D}* to promote prostate neoplasia (14), confirming that apical-basal polarity provides a tumor suppressive barrier that constrains epithelial tumorigenesis (7). In this study, we employed the *Scrib^{Flox}* strain to determine the influence of *Scrib* ablation in PDAC progression. First, we confirmed that *Pdx1^{Cre}; Scrib$^{Flox/Flox}$* mice with targeted deletion of *Scrib* in the pancreas developed normally and showed a histologically normal pancreatic parenchyma (Supplementary Fig. 1A-F). Next, to assess the impact of *Scrib* inactivation on *Kras^{G12D}*-mediated PanIN development and PanIN-to-PDAC progression, we used a well-established PanIN mouse model (25), *Kras$^{LSL-G12D/+}$; Pdx1^{Cre}* (hereinafter referred to as KPdx1). We crossed KPdx1 mice into the *Scrib^{Flox}* strain to generate a cohort of mice in which endogenous *Kras^{G12D}* expression and concomitant monoallelic (*Kras$^{LSL-G12D/+}$; Pdx1^{Cre}; Scrib$^{Flox/+}$* (KPdx1S$^{F/+}$)) or biallelic (*Kras$^{LSL-G12D/+}$; Pdx1^{Cre}; Scrib$^{Flox/Flox}$* (KPdx1S$^{F/F}$)) ablation of *Scrib* were directed to the embryonic pancreas using the *Pdx1^{Cre}* allele (Supplementary Fig. 2A). Mice were monitored until the development of clinical deterioration, and tissue sections were examined histopathologically for grade of PanIN lesions, PDAC and metastatic deposits. We found that neither monoallelic nor biallelic ablation of *Scrib* shortened survival compared to KPdx1 mice (Fig. 1A). *Scrib*-deficient mice consistently

presented the established PanIN-to-PDAC progression sequence observed in KPdx1 mice (25) (Fig. 1B), with young mice exhibiting acinar-to-ductal metaplasia and low grade PanIN lesions that progressed to high grade PanIN lesions and invasive PDAC as the mice aged (Fig. 1C-H, Supplementary Table 2). Overall, *Scrib*-deficient mice did not exhibit a significant increase of PDAC incidence in this background (Supplementary Table 3). However, an accurate evaluation of the impact of *Scrib* deficiency on PanIN-to-PDAC progression was precluded by the premature death of a noteworthy number of mice due to development of infected benign cutaneous papillomas, liver injury and diverse neoplasias (Supplementary Fig. 2B-F; Supplementary Table 2), as a result of the extra-pancreatic expression of the *Pdx1* promoter (25).

To circumvent the effect of this early lethality in our study, we generated a second cohort of mice in which *Scrib* ablation was driven by the more pancreas-specific *Ptf1α/P48* promoter (25) (Supplementary Fig. 1A-D, Supplementary Fig. 3A). As expected, $Kras^{LSL\text{-}G12D/+}$; $Ptf1a/P48^{Cre/+}$ (hereinafter referred to as KP48) mice presented extended survival rate (Fig. 1I) compared to KPdx1 animals (Fig. 1A), which was associated with the drastic reduction of extra-pancreatic phenotypes in KP48 mice (Supplementary Table 4). The analysis of this cohort showed that neither monoallelic ($Kras^{LSL\text{-}G12D/+}$; $Ptf1a/P48^{Cre/+}$; $Scrib^{Flox/+}$ ($KP48S^{F/+}$)) nor biallelic ($Kras^{LSL\text{-}G12D/+}$; $Ptf1a/P48^{Cre/+}$; $Scrib^{Flox/Flox}$ ($KP48S^{F/F}$)) ablation of *Scrib* significantly decreased survival compared to KP48 mice (Fig. 1I). Histological analysis confirmed that ~70% of mice in this cohort developed well-differentiated PDAC, with the remaining animals showing complete replacement of the pancreatic parenchyma by extensive PanIN lesions of different grade surrounded by fibrous stroma (Fig. 1J; Supplementary Fig. 3B-C). Further histological evaluation showed that *Scrib* deficiency did not affect the metastatic potential in this background (Fig. 1J; Supplementary Fig. 3D; Supplementary Table 4).

Collectively, the analysis of these PanIN mouse models showed that inactivation of *Scrib* in pancreatic progenitor cells does not promote neither PanIN formation nor PanIN-to-PDAC progression in a $Kras^{G12D}$ background, strongly suggesting that *Scrib* deficiency does not play a relevant role in early stages of PDAC development.

Loss of *Scrib* cooperates with $Kras^{G12D}$ and monoallelic inactivation of *Trp53* to shorten PDAC-associated survival in mice.

Altered expression of SCRIB is frequently associated with a variety of human neoplasias (14,15,17,21,22). Since *Scrib* deficiency does not seem to influence early stages of pancreatic cancer development (Fig. 1), we speculated that SCRIB may serve as a tumor suppressor in advanced PDAC. To test this hypothesis, we utilized the well-validated $Kras^{LSL\text{-}G12D/+}$; $Trp53^{Flox/+}$; $Pdx1^{Cre}$ (hereinafter referred to as $KP^{F/+}C$) mouse model of PDAC, in which endogenous $Kras^{G12D}$ and concomitant heterozygous inactivation of *Trp53* cooperate to accelerate progression from preinvasive PanIN lesions to invasive PDAC (34).

We generated a cohort of mice in which *Pdx1*^{Cre}-mediated expression of *Kras*^{G12D} and heterozygous inactivation of *Trp53* were combined with monoallelic (*Kras*$^{LSL\text{-}G12D/+}$*; Trp53*$^{Flox/+}$*; Pdx1*^{Cre}*; Scrib*$^{Flox/+}$ (KP$^{F/+}$CS$^{F/+}$)) or biallelic (*Kras*$^{LSL\text{-}G12D/+}$*; Trp53*$^{Flox/+}$*; Pdx1*^{Cre}*; Scrib*$^{Flox/Flox}$ (KP$^{F/+}$CS$^{F/F}$)) ablation of *Scrib* in pancreatic progenitor cells (Supplementary Fig. 4A). Intriguingly, *Scrib* homozygous KP$^{F/+}$CS$^{F/F}$ mice exhibited faster clinical deterioration and accelerated PDAC development compared to *Scrib* heterozygous KP$^{F/+}$CS$^{F/+}$ and *Scrib* wild-type KP$^{F/+}$C counterparts (Fig. 2A). We verified that mice with pancreatic deletion of *Scrib* and concomitant heterozygous inactivation of *Trp53*, in a wild-type *Kras* background (P$^{F/+}$CS$^{F/F}$), developed normally and exhibited standard survival rate (Fig. 2A). Macroscopic analysis of mice at necropsy revealed that KP$^{F/+}$CS$^{F/F}$ animals developed large locally invasive multinodular solid tumors (Fig. 2B). qPCR and western blot analyses showed that pancreatic tumors arisen in *Scrib* heterozygous KP$^{F/+}$CS$^{F/+}$ mice retained the expression of the wild-type *Scrib* allele and, as expected (35), loss of wild-type p53 expression was a general genetic event observed in KP$^{F/+}$C, KP$^{F/+}$CS$^{F/+}$ and KP$^{F/+}$CS$^{F/F}$ PDAC cells (Fig. 2C-D).

Histological examination revealed that tumors developed in KP$^{F/+}$CS$^{F/F}$ mice resembled the histopathological features of human PDAC, showing the classical PanIN-to-PDAC progression cascade (3). Histochemical analysis of low-grade PanIN1 lesions detected cytoplasmic mucin and membranous E-Cadherin expression (Fig. 2E-G), confirming the epithelial nature of PanIN lesions. PanIN1 lesions subsequently progressed to high-grade PanIN3 lesions (Fig. 2H) and, ultimately, to invasive PDAC (Fig. 2I-J). Histologically, tumors displayed high intra-tumoral heterogeneity, with areas of well-differentiated and poorly-differentiated adenocarcinoma within the same tumor (Fig. 2K-L). Remarkably, *Scrib*-null KP$^{F/+}$CS$^{F/F}$ PDAC presented a higher histological grade compared to *Scrib*-expressing KP$^{F/+}$C counterparts (Fig. 2M; Supplementary Fig. 4B), which was associated with loss of cell polarity, denoted by mislocalization (well-differentiated areas) or mislocalization and downregulation (poorly-differentiated areas) of E-Cadherin (Fig. 2N-O).

In summary, the analysis of *Kras*^{G12D}-driven PanIN and PDAC mouse models supports a tumor-suppressive function of SCRIB in advanced stages of pancreatic cancer development.

Scrib deficiency enhances tumor metastasis in the context of _Kras_^{G12D} expression and concomitant heterozygous deletion of _Trp53_.

Distant metastases are the primary cause of death in patients with PDAC (1). To shed light into the cause of the earlier death of *Scrib*-null KP$^{F/+}$CS$^{F/F}$ mice, we examined the influence of *Scrib* deficiency on the metastatic behavior of PDAC tumors. Crucially, *Trp53*-heterozygous KP$^{F/+}$C mice develop PDAC with lower metastatic burden compared to mice harboring mutant *Trp53* alleles (34-36), offering a valuable platform to evaluate genetic events that enhance PDAC dissemination.

Histological analysis showed that 57.1% of *Scrib*-expressing KP$^{F/+}$C mice presented metastatic deposits, generally micrometastases. Remarkably, *Scrib*-null KP$^{F/+}$CS$^{F/F}$ mice developed a widely disseminated disease with metastatic deposits, largely macrometastases, found in 92.3% of animals (*P*

= 0.0139; Fisher's exact test) (Fig. 3A, Supplementary Table 5). A detailed assessment of the metastatic pattern revealed that 73% of $KP^{F/+}CS^{F/F}$ mice developed macroscopic metastases in the lungs, liver and, predominantly, peritoneal cavity (Fig. 3B-F, Supplementary Fig. 5A-C). In contrast, most metastatic deposits in $KP^{F/+}C$ littermates were microscopic, with just 21.4% of animals presenting evident metastases in the liver and peritoneal cavity (Fig. 3C-D, Supplementary Fig. 5D). Notably, *Scrib* inactivation enhanced the development of metastasis in the peritoneum, with 84.6% of $KP^{F/+}CS^{F/F}$ animals presenting metastatic deposits in the peritoneal cavity, compared to 42.8% of $KP^{F/+}C$ counterparts (*P* = 0.0108; Fisher's exact test) (Fig. 3D, Supplementary Fig. 5C-D). A trend toward increased metastatic behavior was observed in the *Scrib*-heterozygous $KP^{F/+}CS^{F/+}$ cohort, with 80.9% of mice showing metastatic deposits (Fig. 3A), and 52.3% of animals presenting macrometastases in the lungs, liver and peritoneal cavity (Fig. 3B-D, Supplementary Fig. 5E, Supplementary Table 5). Concordantly, metastatic deposits in the peritoneum of $KP^{F/+}CS^{F/+}$ mice were less numerous and smaller than those observed in $KP^{F/+}CS^{F/F}$ animals (Fig. 3D, Supplementary Fig. 5C, E) reflecting the incomplete *Scrib* deficiency.

Collectively, these findings establish that *Scrib* deficiency works synergistically with $Kras^{G12D}$ and monoallelic loss of *Trp53* to exacerbate peritoneal dissemination, which likely contributes to the shortened survival of $KP^{F/+}CS^{F/F}$ mice.

Scrib ablation reduces collagen content and fibroblast activation.

PDAC is characterized by a dense extracellular matrix (ECM), of which collagens are principal components (37). The role of the PDAC-associated desmoplastic microenvironment is controversial, with studies showing either pro-tumorigenic (30,38) or anti-tumorigenic (39-42) effects. To interrogate whether the enhanced invasiveness exhibited by *Scrib*-null $KP^{F/+}CS^{F/F}$ tumors was associated with changes in collagen content, we evaluated the collagen network using Sirius Red staining in tumors collected from mice close to humane endpoint. Notably, we found that $KP^{F/+}CS^{F/F}$ tumors showed a significant reduction in collagen fibers, with thin fibers sparsely disseminated, compared to *Scrib*-expressing ($KP^{F/+}C$) counterparts (Fig. 4A-C). Quantitative qPCR analysis confirmed the significant downregulation of *Col1a1* and *Col3a1* in $KP^{F/+}CS^{F/F}$ PDAC (Fig. 4D-E). Based on the reduced collagen content detected in $KP^{F/+}CS^{F/F}$ PDAC, we investigated whether *Scrib* ablation affected fibroblast composition in the tumor stroma. Immunohistochemical analysis showed reduced expression of the pan-fibroblast marker Podoplanin (PDPN) (33) (Fig. 4F-H) and the myofibroblastic CAF marker α-smooth muscle actin (α-SMA) (Fig. 4I-K) in $KP^{F/+}CS^{F/F}$ tumors compared to $KP^{F/+}C$ counterparts. Consistent with these findings, CAF markers such as *Acta2* (coding for α-SMA), *Fap* and *Sparc* were found to be significantly downregulated in $KP^{F/+}CS^{F/F}$ PDAC compared to *Scrib*-expressing $KP^{F/+}C$ tumors (Fig. 4L-N). Collectively, these observations indicate that *Scrib* deficiency leads to a significant reduction in collagen deposition and CAF abundance in PDAC.

To identify molecular and cellular mechanisms involved in this phenotype, we investigated gene expression changes associated with *Scrib* ablation. By employing RNA-seq, we analysed the

transcriptome of $KP^{F/+}C$ and $KP^{F/+}CS^{F/F}$ primary tumors (Supplementary Fig. 6, Supplementary Tables 6-7). In accordance with our findings (Fig. 4), differential expression analysis and Gene Set Enrichment Analysis (GSEA) revealed that $KP^{F/+}CS^{F/F}$ tumors exhibited a significant downregulation of both myCAF and iCAF signatures (Fig. 5A-B), with reduced expression of myCAF (Supplementary Fig. 7A-B) and iCAF (Supplementary Fig. 7C-D) markers (33) in *Scrib*-null $KP^{F/+}CS^{F/F}$ tumors compared to $KP^{F/+}C$ counterparts.

To unveil molecular cues driving the reduced fibroblast content in *Scrib*-null PDAC, we examined the impact of *Scrib* deficiency in the expression of *Il1a* and *Tgfb1*, coding for interleukin 1α (IL1α) and transforming growth factor β1 (TGFβ1), two cancer cell-secreted cytokines that have been shown to be the main mediators of iCAF and myCAF formation, respectively (43). Although bulk transcriptome analysis found no detectable changes in *Il1a* and *Tgfb1* expression between $KP^{F/+}C$ and $KP^{F/+}CS^{F/F}$ tumors (Supplementary Fig. 7E-F), we evaluated whether *Scrib* inactivation altered the expression of *Il1a* and *Tgfb1* in tumor cells. To do this, we knocked down *Scrib* in $KRAS^{G12D}$; p53-deficient mouse $KP^{F/F}C$ PDAC organoids (mPDOs). shScrib mPDOs showed a significant downregulation of *Il1a* compared to shRenilla mPDOs, while *Tgfb1* expression was not affected (Fig. 5C). ELISA of conditioned media from shRenilla and shScrib mPDOs verified that the reduction of *Il1a* RNA level was associated with diminished IL1α protein secretion in shScrib mPDOs (Fig.5D). Immunohistochemical analysis confirmed the *in vivo* reduction of IL1α in *Scrib*-null PDAC compared to *Scrib*-expressing tumors (Fig. 5E-G). Collectively, these data suggest that *Scrib* inactivation may decrease iCAF formation by reducing IL1α expression in tumor cells.

Subsequently, we employed a well-validated 3D *in vitro* approach (27,43) to evaluate the impact of *Scrib* deficiency on iCAF induction. As previously reported (43), PSCs cultured in conditioned media (CM) from mPDOs showed upregulation of iCAF markers (*Il6*, *Il1a*, *Csf3*, *Cxcl1* and *Lif*), downregulation of myCAF markers (*Acta2* and *Ctgf*) and increased expression of the proliferation marker *Mki67* compared to quiescent PSCs cultured in control media (Fig. 5H-I). Strikingly, PSCs cultured in CM from shScrib mPDOs exhibited significant downregulation of iCAF markers and *Mki67* compared to PSCs cultured in CM from shRenilla mPDOs (Fig. 5H-I). These results confirm that *Scrib* deficiency in PDAC cells decreases iCAF activation. Next, to determine whether this diminished iCAF induction was mediated by the reduced IL1α levels exhibited by *Scrib*-deficient mPDOs, we cultured PSCs in CM from shScrib mPDOs in the presence or absence of IL1α. Addition of IL1α to shScrib mPDOs-conditioned media significantly increased the expression of iCAF markers (Fig. 5J), supporting that downregulation of IL1α in *Scrib*-deficient PDAC cells reduces iCAF formation.

To better understand the reduction in myCAFs, we further analysed the tumor transcriptomes of *Scrib*-null $KP^{F/+}CS^{F/F}$ PDACs. Hedgehog signalling has been shown to be more highly activated in myCAFs compared to iCAFs (44). We found that the Hedgehog ligand *Ihh* as well as the Hedgehog transcriptional effectors *Gli1* and *Gli2* were significantly downregulated in *Scrib*-null $KP^{F/+}CS^{F/F}$ tumors compared to *Scrib*-proficient PDAC (Fig. 5K-L), supporting the notion that Hedgehog activity is impaired in $KP^{F/+}CS^{F/F}$ PDAC. Since the Hedgehog ligand IHH has been shown to be expressed by PDAC cells,

whereas the expression of Hedgehog targets, such as *Gli1* and *Gli2*, is constrained to fibroblasts, principally myCAFs (44,45), our data suggest that downregulation of Hedgehog signaling in *Scrib*-deficient tumors may have a role in the observed reduction of myCAFs.

Collectively, our findings support that changes in the cancer cell secretome are responsible for the reduction in iCAFs and myCAFs observed in *Scrib*-null tumors.

***Scrib* deficiency promotes survival of PDAC cells.**

We then investigated cell intrinsic mechanisms that could drive the exacerbated PDAC development observed in *Scrib*-deficient mice. Resistance to detachment-induced apoptosis (anoikis) is a hallmark of cancer progression and promotes survival of tumor cells during metastatic dissemination (46,47). Consequently, we investigated whether *Scrib* downregulation rendered PDAC cells more resistant to anoikis. First, we generated two independent *Scrib*-expressing $KP^{F/+}C$ cell lines expressing either a shRNA against *Scrib* or a control shRNA targeting *Renilla*. Then, shScrib $KP^{F/+}C$ and shRenilla $KP^{F/+}C$ cells were cultured in suspension for 48 hours. *Scrib*-deficient PDAC cells exhibited reduced Caspase-3/7 activity after loss of cellular attachment compared to shRenilla $KP^{F/+}C$ counterparts, while changes in two-dimensional cultures were not observed (Fig. 6A-B). These results sustain the notion that SCRIB deficiency exacerbates PDAC dissemination, as evidenced by increased peritoneal metastasis (Fig. 3D-F), through enhancing resistance to anoikis.

To reveal the molecular basis for the aggressive phenotype of *Scrib*-deficient PDAC cells, we employed RNA-seq to analyze the transcriptome of mPDOs with or without *Scrib* depletion. GSEA revealed that *Scrib* knockdown downregulated the apoptosis signature and upregulated cell cycle progression signatures, including G2M checkpoint, E2F targets and MYC targets, in mPDOs (Fig. 6C-D, Supplementary Fig. 8A-C, Supplementary Tables 8-9). Furthermore, bulk transcriptome analysis found no difference in the apoptosis signature (Supplementary Fig. 9A) and upregulation of genes and signatures related to cell cycle progression (Supplementary Fig. 9B-G) in *Scrib*-null tumors compared to *Scrib*-expressing PDAC. Immunohistochemical analyses showed no changes in Cleaved Caspase-3 (apoptosis marker), but higher Ki67 proliferation index, in $KP^{F/+}CS^{F/F}$ tumors compared to $KP^{F/+}C$ counterparts (Supplementary Fig. 9H-K), supporting the transcriptome analysis in PDAC. Altogether, these findings strongly suggest that *Scrib* deficiency promotes cell cycle progression and protects tumor cells from apoptotic stimuli such as loss of cellular attachment, verifying the tumor suppressor activity of SCRIB in PDAC malignant cells.

To shed light on the molecular mechanisms by which *Scrib* loss enhances PDAC cell aggressiveness, we focused on YAP/TAZ, two Hippo pathway transcriptional regulators that promote cell survival in PDAC (48,49) and have been shown to be negatively regulated by SCRIB in human cancer cells (50-54). We found that *Scrib* knockdown increased active YAP protein levels in mPDOs, as assessed by western blot for the active (non-phosphorylated) YAP isoform (Fig. 6E-F). Furthermore, active YAP levels were significantly upregulated in *Scrib*-null $KP^{F/+}CS^{F/F}$ tumors compared to *Scrib*-expressing

counterparts (Fig. 6G-H). Finally, we observed that *Scrib*-deficient mPDOs exhibited enhanced cell viability compared to shRenilla mPDOs in the presence of the YAP inhibitor Verteporfin (Fig. 6I-J). Taken together, these data suggest that activation of YAP upon *Scrib* downregulation promotes survival of PDAC cells.

SCRIB expression is altered in human PDAC and determines clinical outcome.

To determine the relevance of SCRIB in human PDAC, we assessed by immunohistochemistry the expression of SCRIB in normal, preneoplastic and neoplastic pancreatic tissues. SCRIB was highly expressed at the cell-cell junctions in normal pancreatic ducts (Fig. 7A). In PanIN lesions with mild to moderate grade of cellular atypia, cell polarity is largely maintained and SCRIB exhibits membranous localization (Fig. 7B-C). Well-differentiated PDAC lesions displayed a mixed pattern, with some glandular lesions showing predominant membranous SCRIB staining, and other regions displaying cytoplasmic staining (Fig. 7D). Finally, SCRIB was found to be largely downregulated and/or mislocalized in moderately-differentiated and poorly-differentiated PDAC (Fig. 7E-F). Collectively, these findings suggest that disruption of epithelial integrity in PDAC is associated with dysregulation of SCRIB by downregulation and/or mislocalization.

Next, we investigated in a cohort of 196 patients who underwent tumor resection for localized PDAC, whether SCRIB levels in primary tumours were associated with median survival after surgery. Immunohistochemical analysis determined that SCRIB protein was strongly downregulated in PDAC compared to normal pancreatic tissue (Fig. 7G). Kaplan-Meier analysis showed a trend toward reduced survival in patients with low expression of SCRIB compared to patients expressing medium and high levels of SCRIB (Fig. 7H). Since SCRIB mislocalization has been associated with tumor progression (20,22), we assessed whether SCRIB localization determined PDAC outcome in a cohort of 179 patients who underwent surgical resection of PDAC. Remarkably, we found a strong association between SCRIB localization and surgical margin status on the survival outcome after resection. Indeed, Kaplan-Meier analyses exposed that while subcellular localization of SCRIB did not affect survival in patients with negative resection margins (Fig. 7I), cytoplasmic SCRIB staining was strongly associated with shorter median survival, compared to membranous SCRIB staining, in the group of patients with positive surgical margins (Fig. 7J). Collectively, these data support that cytoplasmic mislocalization of SCRIB plays a relevant role in the pathogenesis of PDAC.

To evaluate the relevance of the subcellular localization of SCRIB on the neoplastic properties of human PDAC cells, we first appraised the levels of SCRIB in a panel of well-characterized human PDAC cell lines and found variable expression across them (Supplementary Fig. 10A). Next, we selected one cell lines with low SCRIB expression, CFPAC1, for additional studies. We ectopically expressed $SCRIB^{WT}$ (membranous localization) and $SCRIB^{P305L}$, a mutant isoform that fails to localize to the plasma membrane (20), in CFPAC1 cells (Fig. 8A, Supplementary Fig. 10B). We found that ectopic expression of membranous $SCRIB^{WT}$ significantly diminished viability when cells were cultured in reduced growth factor media (Fig. 8B), and drastically reduced the ability to form foci under confluent culture conditions

(Supplementary Fig. 10C-F), compared to CFPAC1 cells transduced with an empty vector. Furthermore, ectopic SCRIB^{WT} increased Caspase-3/7 activity when cells were grown in suspension, but no in two-dimensional cultures (Fig. 8C), strengthening our findings in mouse PDAC cells (Fig. 6A-B) that suggested that SCRIB deficiency increases resistance to anoikis. Overall, these data support the tumor suppressor role of membranous SCRIB in PDAC. Notably, ectopic expression of the cytoplasmic SCRIB^{P305L} isoform was unable to diminish the transformed phenotype of CFPAC1 cells (Fig. 8B-C, Supplementary Fig. 10C-F), confirming that mislocalization of SCRIB disrupts its tumor-suppressive properties, and reinforcing our observations in human PDAC (Fig. 7J).

Cytoplasmic localization of SCRIB has been associated to the activation of the Hippo transducers YAP and TAZ in diverse neoplastic cells (50,52-54). However, the impact of SCRIB mislocalization in the regulation of the YAP/TAZ pathway in human PDAC cells has not been illustrated yet. We found that CFPAC1 cells expressing cytoplasmic SCRIB^{P305L} (CFPAC1-SCRIB^{P305L}) showed higher levels of active YAP and TAZ (Fig. 8D-F), and increased YAP/TAZ reporter activity (Fig. 8G), compared to cells expressing membranous SCRIB (CFPAC1-SCRIB^{WT}). Furthermore, CFPAC1-SCRIB^{P305L} cells exhibited enhanced resistance to YAP inhibition compared to CFPAC1-SCRIB^{WT} cells, denoted by the ability to form foci when cells were cultured under confluent conditions in the presence of the YAP inhibitor Verteporfin (Fig. 8H-I).

Finally, we knocked down *SCRIB* in a human PDAC cell line expressing relatively high level of SCRIB, PATU8902 (Supplementary Fig. 10A). We found that *SCRIB* knockdown upregulated active YAP and TAZ levels (Supplementary Fig. 11A-C), and this was associated with increased resistance to Verteporfin (Supplementary Fig. 11D). Moreover, *SCRIB* dowregulation reduced Caspase-3/7 activity when cells were grown in suspension, but no in two-dimensional cultures (Supplementary Fig. 11E).

Collectively, these data support the tumor suppressor activity of SCRIB and confirm the biological significance of activated YAP/TAZ in PDAC cells with altered expression of SCRIB, strengthening our previous findings in mPDOs (Fig. 6I-J), and supporting that dysregulation of the YAP/TAZ pathway may play a relevant role in the enhanced transformed phenotype observed in SCRIB-defective cells.

DISCUSSION

Robust evidence indicates that cell polarity disruption plays a pivotal role during the initiation, progression and metastatic spread of epithelial neoplasias (6,7). This is particularly evident in PDAC, where perturbation of the apical-basal polarity is progressively worsened from low-grade PanIN lesions to invasive PDAC (3). The role of SCRIB in cancer development is complex and context dependent. While SCRIB is downregulated and acts as tumor suppressor in diverse human epithelial neoplasias (14,15,17), certain tumors exhibit increased levels of SCRIB, usually associated with cytoplasmic mislocalization (17,20-22). Thus, SCRIB has the potential to function as an oncogene when is not

located in the membrane. Importantly, the tumor suppressor (14-18) and oncogenic (19,20) activities of SCRIB have been confirmed in mouse models of cancer. In this study, we have used well-validated mouse models of pancreatic cancer to show that *Scrib* inactivation cooperates with oncogenic *Kras*^{G12D} and *Trp53* heterozygosity to accelerate tumor development and severely enhance metastatic dissemination, supporting a tumor suppressor role of SCRIB in advanced PDAC.

Employing a genetically unbiased transposon-mediated insertional mutagenesis approach in a KRAS^{G12D}-driven PanIN mouse model, we previously identified recurrent alterations of polarity genes during PanIN-to-PDAC progression (55). Notably, mutations in genes coding for apical-basal polarity regulators were found in over 36% of the tumors (Supplementary Fig. 12), reinforcing the notion that perturbation of apical-basal polarity signaling is a crucial event in PDAC development. Strikingly, *Scrib* was not found to be mutated in this screen, supporting findings of this study that show that *Scrib* inactivation is not an essential genetic event during early stages of PDAC development. Interestingly, monoallelic inactivation of *Scrib* drives prostate and lung hyperplasia, and cooperates with *Kras*^{G12D} to accelerate prostate and lung cancer (14,15), giving evidence that the tumor suppressor activity of SCRIB depends on both the genetic and cellular contexts. More generally, our study sheds light on the context dependent activity of polarity regulators during the different stages of tumor development.

Using a mouse model of accelerated PDAC progression (*Kras*$^{LSL\text{-}G12D/+}$*; Trp53*$^{Flox/+}$*; Pdx1*^{Cre}), we reveal that *Scrib* inactivation synergizes with *Kras*^{G12D} expression and concomitant heterozygous inactivation of *Trp53* to accelerate PDAC development and exacerbate metastatic dissemination. Interestingly, SCRIB deficiency increases resistance to anoikis in PDAC cells, supporting the notion that the tumor suppressive activity of SCRIB is mediated, in part, by regulating apoptosis. This aligns with previous findings by Zhan and colleagues that showed that inactivation of *Scrib* cooperates with c-MYC to drive breast cancer by inhibiting apoptosis (17). Furthermore, we find that altered expression of SCRIB increases the levels of the Hippo transducers YAP/TAZ in mPDOs and human PDAC cells, and SCRIB-deficient cells exhibit enhanced resistance to the antiproliferative activity of the YAP inhibitor Verteporfin. These findings reinforce the role of the YAP/TAZ pathway in cell survival and PDAC progression (48,49,56,57), and further support previous observations demonstrating that SCRIB regulates the YAP/TAZ pathway in other malignancies (50-54), thus proposing the dysregulation of the SCRIB-YAP/TAZ axis as a relevant player in the pathogenesis of PDAC.

In addition to cell intrinsic changes, *Scrib*-null tumors exhibit a marked depletion of CAFs accompanied with a significant reduction of collagen content. Although further investigation will be needed to fully elucidate the precise role of CAFs in the aggressive behavior of SCRIB-defective PDAC cells, these findings are in accord with previous studies indicating that reduced fibrosis and CAF content can promote tumor development, invasion and metastasis in PDAC (39-42), and is associated with worse clinical outcome (58-60). We show that IL1α, a key cancer cell-secreted ligand responsible for iCAF induction (43), is downregulated in *Scrib*-deficient mPDOs, and this is associated with less activation of PSCs into iCAFs. In tumors, IL1α protein level, but not *Il1a* mRNA, is reduced in *Scrib*-null PDAC, suggesting that post-transcriptional mechanisms regulate IL1α expression. Overall, our data propose

that inactivation of the SCRIB-IL1α axis may play an important function in the reduced CAF content of *Scrib*-null PDAC. Moreover, transcriptome analyses reveal that *Scrib* ablation decreases Hedgehog signaling in PDAC. Hedgehog signaling has been shown to be confined to the fibroblast compartment in PDAC, with paracrine mechanisms driven by PDAC cell-secreted Hedgehog ligands inducing the activation of CAFs, predominantly myCAFs (44,45). Accordingly, our findings support the idea that the reduced Hedgehog signaling exhibited by *Scrib*-deficient tumors may have a role in the reduced myCAF activation observed, and validate previous findings by Rhim and colleagues that showed that *Shh* loss accelerated PDAC development, with tumors presenting a reduced myofibroblast content (39). Overall, our data provide insight into the regulation of the tumor microenvironment during PDAC development. We propose that genetic events leading to a remodeling and partial reduction of the dense fibrotic stroma surrounding neoplastic cells in established tumors will create a more permissive environment for PDAC invasion and dissemination. Therefore, identification of key PDAC metastatic drivers will lead to a better understanding of critical aspects of the metastatic process and will provide new prognostic biomarkers for better patient stratification.

Analyses of human PDAC specimens have reinforced the findings obtained in mouse models. SCRIB is expressed in the plasma membrane of human PanIN lesions, and downregulated and/or mislocalized in human PDAC, supporting the notion that perturbation of physiological SCRIB activity is a late event during pancreatic cancer development. Strikingly, the analysis of a cohort of patients with resected PDAC showed that cytoplasmic expression of SCRIB is associated with worse prognosis in patients with positive surgical margins. Notably, our data support previous studies that revealed the oncogenic activity of cytoplasmic SCRIB in breast and liver cancers (17,20,22), and implicate cytoplasmic localization of SCRIB as a relevant driver of human pancreatic cancer development.

In summary, we reveal that *Scrib* deficiency cooperates with $Kras^{G12D}$ and heterozygous inactivation of *Trp53* to accelerate PDAC development and exacerbate peritoneal dissemination. This enhanced aggressive behavior is mediated via both cell-autonomous and non-cell autonomous mechanisms. We show that defective expression of SCRIB correlates with worse prognosis in PDAC and validate the clinical relevance of SCRIB alteration in human PDAC. We therefore propose that the apical-basal polarity regulator SCRIB is a tumor suppressor in advanced pancreatic cancer with clinical significance. Since peritoneal dissemination is observed in around 50% of patients with pancreatic cancer and is associated with poor prognosis (1,47), further investigation to selectively target each CAF population will be needed to elucidate the role of CAFs in the invasive phenotype of SCRIB-deficient PDAC.

Acknowledgements: We thank A. Gopinathan, F. Connor and other members of Tuveson's and Perez-Mancera's labs for assistance and advice. We thank Prof Eithne Costello, Prof Bill Greenhalf, Prof Paula Ghaneh, Prof John Neoptolemos, Prof Robert Sutton, Prof Chris Goldring, Dr Carlos Rubbi and James Miller for continuous support. We thank Dr Johannes Zuber for kindly providing the LENG and LEPG vectors and Eloise Lloyd for technical advice with ELISAs. We also acknowledge the Biomedical Research Unit and Histology, Genomics, Bioinformatics and Research Instrumentation and Cell Services core facilities at the Cancer Research UK Cambridge Institute, and the Biomedical Services Unit, Centre for Cell Imaging and Biobank at the University of Liverpool. P.A. Perez-Mancera is supported by The Hampson Legacy Trust (A0873/CF), NC3Rs (NC/V001167/1) and the University of Liverpool. D.A. Tuveson is a distinguished scholar and Director of the Lustgarten Foundation–designated Laboratory of Pancreatic Cancer Research. D.A. Tuveson is supported by the Cold Spring Harbor Laboratory and Northwell Health Affiliation, and the National Institutes of Health (5P30CA45508, R01CA249002, U01CA224013, U01CA210240 and 1R01CA188134). G. Biffi is a recipient of a UKRI Future Leaders Fellowship and is supported by a Cancer Research UK institutional grant (A27463), the Royal Society, the Pancreatic Cancer Research Foundation, the Wellcome Isaac ISSF/University of Cambridge joint grant and the Pancreatic Cancer and CMB Programmes at the CRUK Cambridge Centre. M. Narita and M. Narita are supported by Cancer Research UK Cambridge Institute Core Grant (C9545/A29580). A. Neesse is supported by a Max Eder Fellowship of the German Cancer Aid (70113213). C. Bermejo-Rodriguez is supported by the University of Liverpool, The Hampson Legacy Trust and NC3Rs. J. Araos Henriquez is supported by a Harding Distinguished Postgraduate Programme PhD studentship (Cambridge Trust). Y. Park is supported by NCI R50CA211506. G. Caligiuri is supported by the American Cancer Research Foundation (AICF).

Author Contributions: CB-R performed *in vitro* experiments, designed experiments, analyzed data and wrote the manuscript. JAH and SPT performed *in vitro* experiments with PDAC organoids, RNA-seq experiments and analysis. GC and YP performed *in vivo* experiments and histological analysis. AE, LNB, AN, MN and MN performed data analysis and interpretation. RG, DA, PR, TK, DO and CP generated data from resected pancreatic tumours. FC analyzed mouse pathology. LED and POH created the *Scrib*^{Flox} targeting vector and analyzed data. GB designed the RNA-seq experiments, analyzed the data and wrote the manuscript. DAT conceived the project, analyzed the data and wrote the manuscript. PAP-M conceived the project, performed *in vivo* experiments, analyzed the data and wrote the manuscript. All the authors discussed the results and edited the final manuscript.

BIBLIOGRAPHY

1. Yachida S, Jones S, Bozic I, Antal T, Leary R, Fu B*, et al.* Distant metastasis occurs late during the genetic evolution of pancreatic cancer. Nature **2010**;467:1114-7
2. Kleeff J, Korc M, Apte M, La Vecchia C, Johnson CD, Biankin AV*, et al.* Pancreatic cancer. Nat Rev Dis Primers **2016**;2:16022
3. Hruban RH, Goggins M, Parsons J, Kern SE. Progression model for pancreatic cancer. Clin Cancer Res **2000**;6:2969-72
4. Perez-Mancera PA, Guerra C, Barbacid M, Tuveson DA. What we have learned about pancreatic cancer from mouse models. Gastroenterology **2012**;142:1079-92
5. Feigin ME, Muthuswamy SK. Polarity proteins regulate mammalian cell-cell junctions and cancer pathogenesis. Curr Opin Cell Biol **2009**;21:694-700
6. Muthuswamy SK, Xue B. Cell polarity as a regulator of cancer cell behavior plasticity. Annu Rev Cell Dev Biol **2012**;28:599-625
7. Halaoui R, McCaffrey L. Rewiring cell polarity signaling in cancer. Oncogene **2015**;34:939-50
8. Fomicheva M, Tross EM, Macara IG. Polarity proteins in oncogenesis. Curr Opin Cell Biol **2020**;62:26-30
9. McCaffrey LM, Macara IG. Signaling pathways in cell polarity. Cold Spring Harb Perspect Biol **2012**;4
10. Santoni MJ, Kashyap R, Camoin L, Borg JP. The Scribble family in cancer: twentieth anniversary. Oncogene **2020**;39:7019-33
11. Stephens R, Lim K, Portela M, Kvansakul M, Humbert PO, Richardson HE. The Scribble Cell Polarity Module in the Regulation of Cell Signaling in Tissue Development and Tumorigenesis. J Mol Biol **2018**;430:3585-612
12. Bilder D, Li M, Perrimon N. Cooperative regulation of cell polarity and growth by Drosophila tumor suppressors. Science **2000**;289:113-6
13. Brumby AM, Richardson HE. scribble mutants cooperate with oncogenic Ras or Notch to cause neoplastic overgrowth in Drosophila. EMBO J **2003**;22:5769-79
14. Pearson HB, Perez-Mancera PA, Dow LE, Ryan A, Tennstedt P, Bogani D*, et al.* SCRIB expression is deregulated in human prostate cancer, and its deficiency in mice promotes prostate neoplasia. J Clin Invest **2011**;121:4257-67
15. Elsum IA, Yates LL, Pearson HB, Phesse TJ, Long F, O'Donoghue R*, et al.* Scrib heterozygosity predisposes to lung cancer and cooperates with KRas hyperactivation to accelerate lung cancer progression in vivo. Oncogene **2014**;33:5523-33
16. Godde NJ, Sheridan JM, Smith LK, Pearson HB, Britt KL, Galea RC*, et al.* Scribble modulates the MAPK/Fra1 pathway to disrupt luminal and ductal integrity and suppress tumour formation in the mammary gland. PLoS Genet **2014**;10:e1004323
17. Zhan L, Rosenberg A, Bergami KC, Yu M, Xuan Z, Jaffe AB*, et al.* Deregulation of scribble promotes mammary tumorigenesis and reveals a role for cell polarity in carcinoma. Cell **2008**;135:865-78
18. Pearson HB, McGlinn E, Phesse TJ, Schluter H, Srikumar A, Godde NJ*, et al.* The polarity protein Scrib mediates epidermal development and exerts a tumor suppressive function during skin carcinogenesis. Mol Cancer **2015**;14:169
19. Hawkins ED, Oliaro J, Ramsbottom KM, Newbold A, Humbert PO, Johnstone RW*, et al.* Scribble acts as an oncogene in Emu-myc-driven lymphoma. Oncogene **2016**;35:1193-7
20. Feigin ME, Akshinthala SD, Araki K, Rosenberg AZ, Muthuswamy LB, Martin B*, et al.* Mislocalization of the cell polarity protein scribble promotes mammary tumorigenesis and is associated with basal breast cancer. Cancer Res **2014**;74:3180-94
21. Vaira V, Faversani A, Dohi T, Maggioni M, Nosotti M, Tosi D*, et al.* Aberrant overexpression of the cell polarity module scribble in human cancer. Am J Pathol **2011**;178:2478-83

22. Wan S, Meyer AS, Weiler SME, Rupp C, Toth M, Sticht C*, et al.* Cytoplasmic localization of the cell polarity factor scribble supports liver tumor formation and tumor cell invasiveness. Hepatology **2018**;67:1842-56
23. Jackson EL, Willis N, Mercer K, Bronson RT, Crowley D, Montoya R*, et al.* Analysis of lung tumor initiation and progression using conditional expression of oncogenic K-ras. Genes Dev **2001**;15:3243-8
24. Marino S, Vooijs M, van Der Gulden H, Jonkers J, Berns A. Induction of medulloblastomas in p53-null mutant mice by somatic inactivation of Rb in the external granular layer cells of the cerebellum. Genes Dev **2000**;14:994-1004
25. Hingorani SR, Petricoin EF, Maitra A, Rajapakse V, King C, Jacobetz MA*, et al.* Preinvasive and invasive ductal pancreatic cancer and its early detection in the mouse. Cancer Cell **2003**;4:437-50
26. Kawaguchi Y, Cooper B, Gannon M, Ray M, MacDonald RJ, Wright CV. The role of the transcriptional regulator Ptf1a in converting intestinal to pancreatic progenitors. Nat Genet **2002**;32:128-34
27. Ohlund D, Handly-Santana A, Biffi G, Elyada E, Almeida AS, Ponz-Sarvise M*, et al.* Distinct populations of inflammatory fibroblasts and myofibroblasts in pancreatic cancer. J Exp Med **2017**;214:579-96
28. Oni TE, Biffi G, Baker LA, Hao Y, Tonelli C, Somerville TDD*, et al.* SOAT1 promotes mevalonate pathway dependency in pancreatic cancer. J Exp Med **2020**;217
29. Boj SF, Hwang CI, Baker LA, Chio, II, Engle DD, Corbo V*, et al.* Organoid models of human and mouse ductal pancreatic cancer. Cell **2015**;160:324-38
30. Olive KP, Jacobetz MA, Davidson CJ, Gopinathan A, McIntyre D, Honess D*, et al.* Inhibition of Hedgehog signaling enhances delivery of chemotherapy in a mouse model of pancreatic cancer. Science **2009**;324:1457-61
31. Perez-Mancera PA, Tuveson DA. Physiological analysis of oncogenic K-ras. Methods Enzymol **2006**;407:676-90
32. Fellmann C, Hoffmann T, Sridhar V, Hopfgartner B, Muhar M, Roth M*, et al.* An optimized microRNA backbone for effective single-copy RNAi. Cell Rep **2013**;5:1704-13
33. Elyada E, Bolisetty M, Laise P, Flynn WF, Courtois ET, Burkhart RA*, et al.* Cross-Species Single-Cell Analysis of Pancreatic Ductal Adenocarcinoma Reveals Antigen-Presenting Cancer-Associated Fibroblasts. Cancer Discov **2019**;9:1102-23
34. Bardeesy N, Aguirre AJ, Chu GC, Cheng KH, Lopez LV, Hezel AF*, et al.* Both p16(Ink4a) and the p19(Arf)-p53 pathway constrain progression of pancreatic adenocarcinoma in the mouse. Proc Natl Acad Sci U S A **2006**;103:5947-52
35. Hingorani SR, Wang L, Multani AS, Combs C, Deramaudt TB, Hruban RH*, et al.* Trp53R172H and KrasG12D cooperate to promote chromosomal instability and widely metastatic pancreatic ductal adenocarcinoma in mice. Cancer Cell **2005**;7:469-83
36. Morton JP, Timpson P, Karim SA, Ridgway RA, Athineos D, Doyle B*, et al.* Mutant p53 drives metastasis and overcomes growth arrest/senescence in pancreatic cancer. Proc Natl Acad Sci U S A **2010**;107:246-51
37. Feig C, Gopinathan A, Neesse A, Chan DS, Cook N, Tuveson DA. The pancreas cancer microenvironment. Clin Cancer Res **2012**;18:4266-76
38. Provenzano PP, Cuevas C, Chang AE, Goel VK, Von Hoff DD, Hingorani SR. Enzymatic targeting of the stroma ablates physical barriers to treatment of pancreatic ductal adenocarcinoma. Cancer Cell **2012**;21:418-29
39. Rhim AD, Oberstein PE, Thomas DH, Mirek ET, Palermo CF, Sastra SA*, et al.* Stromal elements act to restrain, rather than support, pancreatic ductal adenocarcinoma. Cancer Cell **2014**;25:735-47
40. Rath N, Morton JP, Julian L, Helbig L, Kadir S, McGhee EJ*, et al.* ROCK signaling promotes collagen remodeling to facilitate invasive pancreatic ductal adenocarcinoma tumor cell growth. EMBO Mol Med **2017**;9:198-218

41. Chugh S, Barkeer S, Rachagani S, Nimmakayala RK, Perumal N, Pothuraju R*, et al.* Disruption of C1galt1 Gene Promotes Development and Metastasis of Pancreatic Adenocarcinomas in Mice. Gastroenterology **2018**
42. Ozdemir BC, Pentcheva-Hoang T, Carstens JL, Zheng X, Wu CC, Simpson TR*, et al.* Depletion of carcinoma-associated fibroblasts and fibrosis induces immunosuppression and accelerates pancreas cancer with reduced survival. Cancer Cell **2014**;25:719-34
43. Biffi G, Oni TE, Spielman B, Hao Y, Elyada E, Park Y*, et al.* IL1-Induced JAK/STAT Signaling Is Antagonized by TGFbeta to Shape CAF Heterogeneity in Pancreatic Ductal Adenocarcinoma. Cancer Discov **2019**;9:282-301
44. Steele NG, Biffi G, Kemp SB, Zhang Y, Drouillard D, Syu L*, et al.* Inhibition of Hedgehog Signaling Alters Fibroblast Composition in Pancreatic Cancer. Clin Cancer Res **2021**;27:2023-37
45. Tian H, Callahan CA, DuPree KJ, Darbonne WC, Ahn CP, Scales SJ*, et al.* Hedgehog signaling is restricted to the stromal compartment during pancreatic carcinogenesis. Proc Natl Acad Sci U S A **2009**;106:4254-9
46. Mehlen P, Puisieux A. Metastasis: a question of life or death. Nat Rev Cancer **2006**;6:449-58
47. Avula LR, Hagerty B, Alewine C. Molecular mediators of peritoneal metastasis in pancreatic cancer. Cancer Metastasis Rev **2020**;39:1223-43
48. Kapoor A, Yao W, Ying H, Hua S, Liewen A, Wang Q*, et al.* Yap1 activation enables bypass of oncogenic Kras addiction in pancreatic cancer. Cell **2014**;158:185-97
49. Zhang W, Nandakumar N, Shi Y, Manzano M, Smith A, Graham G*, et al.* Downstream of mutant KRAS, the transcription regulator YAP is essential for neoplastic progression to pancreatic ductal adenocarcinoma. Sci Signal **2014**;7:ra42
50. Cordenonsi M, Zanconato F, Azzolin L, Forcato M, Rosato A, Frasson C*, et al.* The Hippo transducer TAZ confers cancer stem cell-related traits on breast cancer cells. Cell **2011**;147:759-72
51. Mohseni M, Sun J, Lau A, Curtis S, Goldsmith J, Fox VL*, et al.* A genetic screen identifies an LKB1-MARK signalling axis controlling the Hippo-YAP pathway. Nat Cell Biol **2014**;16:108-17
52. Chen B, Zheng B, DeRan M, Jarugumilli GK, Fu J, Brooks YS*, et al.* ZDHHC7-mediated S-palmitoylation of Scribble regulates cell polarity. Nat Chem Biol **2016**;12:686-93
53. Zhao D, Yin Z, Soellner MB, Martin BR. Scribble sub-cellular localization modulates recruitment of YES1 to regulate YAP1 phosphorylation. Cell Chem Biol **2021**;28:1235-41 e5
54. Adachi Y, Kimura R, Hirade K, Yanase S, Nishioka Y, Kasuga N*, et al.* Scribble mis-localization induces adaptive resistance to KRAS G12C inhibitors through feedback activation of MAPK signaling mediated by YAP-induced MRAS. Nat Cancer **2023**;4:829-43
55. Perez-Mancera PA, Rust AG, van der Weyden L, Kristiansen G, Li A, Sarver AL*, et al.* The deubiquitinase USP9X suppresses pancreatic ductal adenocarcinoma. Nature **2012**;486:266-70
56. Zhang Q, Zhang Y, Parsels JD, Lohse I, Lawrence TS, Pasca di Magliano M*, et al.* Fbxw7 Deletion Accelerates Kras(G12D)-Driven Pancreatic Tumorigenesis via Yap Accumulation. Neoplasia **2016**;18:666-73
57. Gruber R, Panayiotou R, Nye E, Spencer-Dene B, Stamp G, Behrens A. YAP1 and TAZ Control Pancreatic Cancer Initiation in Mice by Direct Up-regulation of JAK-STAT3 Signaling. Gastroenterology **2016**;151:526-39
58. Erkan M, Michalski CW, Rieder S, Reiser-Erkan C, Abiatari I, Kolb A*, et al.* The activated stroma index is a novel and independent prognostic marker in pancreatic ductal adenocarcinoma. Clin Gastroenterol Hepatol **2008**;6:1155-61
59. Wang LM, Silva MA, D'Costa Z, Bockelmann R, Soonawalla Z, Liu S*, et al.* The prognostic role of desmoplastic stroma in pancreatic ductal adenocarcinoma. Oncotarget **2016**;7:4183-94
60. Ashina S, Masuda A, Yamakawa K, Hamada T, Tsujimae M, Tanaka T*, et al.* A comprehensive analysis of tumor-stromal collagen in relation to pathological, molecular, and immune characteristics and patient survival in pancreatic ductal adenocarcinoma. J Gastroenterol **2023**;58:1055-67

FIGURES:

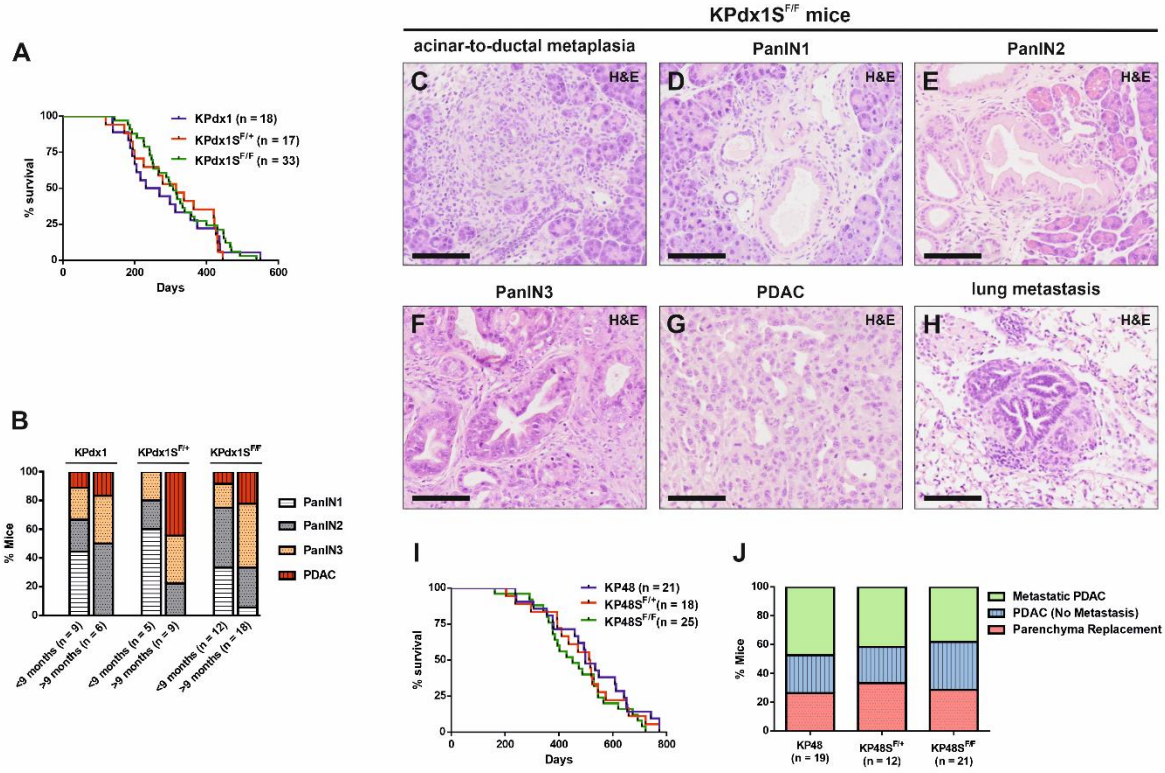

Figure 1

Figure 1. *Scrib* deficiency does not influence PanIN pathogenesis. A, Kaplan-Meier survival curve of KPdx1 mice (250 days) compared to KPdx1S$^{F/+}$ (315 days, P = 0.9693; log-rank test) and KPdx1S$^{F/F}$ (307 days, P = 0.4939; log-rank test) counterparts. **B**, Pancreatic phenotype incidence in KP48, KP48S$^{F/+}$ and KP48S$^{F/F}$ mice deceased before and after 9 months of age. **C-H**, Representative histological sections of acinar-to-ductal metaplasia (**C**), PanIN1 (**D**), PanIN2 (**E**), PanIN3 (**F**), PDAC (**G**) and lung metastasis (**H**) in KPdx1S$^{F/F}$ mice. Scale bars: 100 µm. **I**, Kaplan-Meier survival curve of KP48 mice (498 days) compared to KP48S$^{F/+}$ (514 days, P = 0.6176; log-rank test) and KP48S$^{F/F}$ (451 days, P = 0.1857; log-rank test) counterparts. **J**, Pancreatic phenotype incidence at necropsy in KP48, KP48S$^{F/+}$ and KP48S$^{F/F}$ mice.

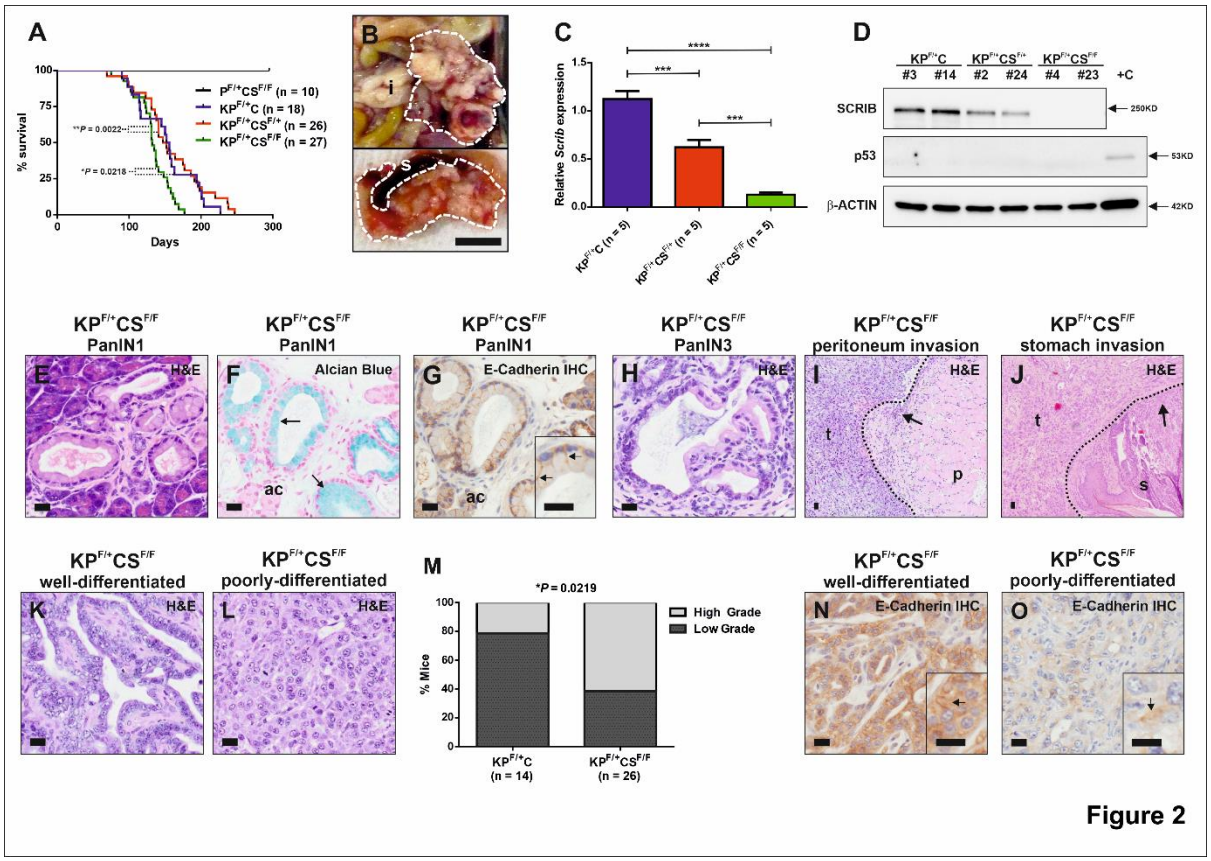

Figure 2. *Scrib* deficiency cooperates with *Kras*^{G12D} and monoallelic inactivation of *Trp53* to promote PanIN-to-PDAC progression. A, Kaplan-Meier survival curve of KP$^{F/+}$CS$^{F/F}$ mice (132 days) compared to KP$^{F/+}$CS$^{F/+}$ (149.5 days, *P* = 0.0022; log-rank test) and KP$^{F/+}$C (154 days, *P* = 0.0218; log-rank test) counterparts. **B**, Gross pathology of KP$^{F/+}$CS$^{F/F}$ pancreata at necropsy. Dashed lines border the primary tumor. i: intestine; s: spleen. Scale bar: 1 cm. **C**, qPCR analysis of *Scrib* in KP$^{F/+}$C, KP$^{F/+}$CS$^{F/+}$ and KP$^{F/+}$CS$^{F/F}$ PDAC. Results show the mean, s.e.m and *P-values* (***P < 0.001, ****P < 0.0001; One-way ANOVA with Bonferroni post-test). **D**, Western blot analysis showing SCRIB and p53 protein expression in primary PDAC cell lines derived from KP$^{F/+}$C, KP$^{F/+}$CS$^{F/+}$ and KP$^{F/+}$CS$^{F/F}$ mice. Wild-type MEFs (+C) are used as positive control of p53. β-ACTIN is used as loading control. **E**, Representative histological section of low-grade PanIN1 lesions. Scale bar: 20 μm. **F**, Alcian blue stain reveals abundant mucin content in PanIN cells (arrows). ac: acinar cells. Scale bar: 20 μm. **G,** Representative immunohistochemical staining of E-Cadherin in PanIN cells (arrows). ac: acinar cells. Scale bar: 20 μm. **H**, Representative histological section of high-grade PanIN3 lesion. Scale bar: 20 μm. **I-J**, Representative histological sections of PDAC invading (arrow) the peritoneum layer (**I**) and stomach (**J**). t: tumor; p: peritoneum layer; s: stomach. Dotted lines indicate the tumor invasive front. Scale bars: 20 μm. **K-L**, Representative histological sections of well-differentiated (**K**) and poorly-differentiated (**L**) areas within a PDAC sample. Scale bars: 20 μm. **M**, Histological grade of tumors developed in KP$^{F/+}$C and KP$^{F/+}$CS$^{F/F}$ mice. Tumors with over 50% area exhibiting well-differentiated or moderately differentiated histological grade were classified as Low Grade, while tumors with over 50% area presenting poorly-differentiated or anaplastic histological grade were classified as High Grade (*P* = 0.0219; Fisher's exact test). **N-O**, Representative immunohistochemical staining of E-Cadherin showing strong and mislocalized expression (arrow) in well-differentiated (**N**), and weak and mislocalized expression (arrow) in poorly-differentiated (**O**) areas within KP$^{F/+}$CS$^{F/F}$ tumors. Scale bars: 20 μm.

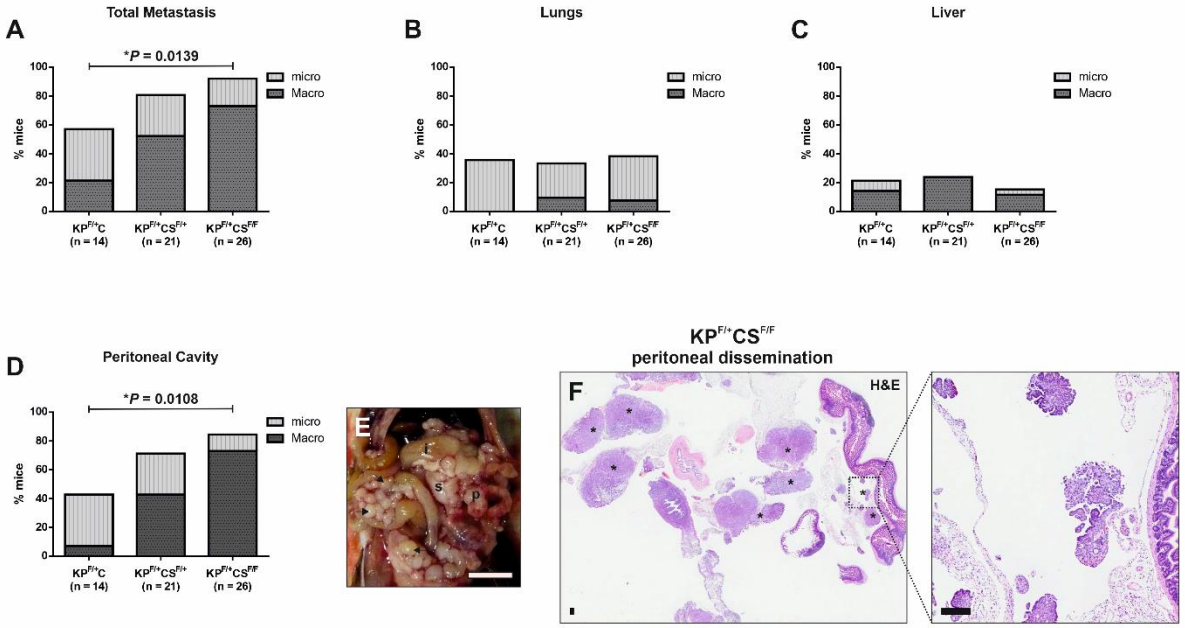

Figure 3

Figure 3. *Scrib* deficiency enhances peritoneal dissemination. A-D, Total metastatic potential (% mice with metastases) (**A**), and metastatic potential to lungs (**B**), liver (**C**) and peritoneal cavity (**D**) in $KP^{F/+}C$, $KP^{F/+}CS^{F/+}$ and $KP^{F/+}CS^{F/F}$ animals. Results show *P-values* (Fisher's exact test). micro: % mice presenting only histologically detected micrometastases; Macro: % mice presenting evident macrometastases at necropsy. **E**, Gross pathology of peritoneal dissemination (arrows) in $KP^{F/+}CS^{F/F}$ mice at necropsy. p: primary tumor; i: intestine; s: stomach. Scale bar: 1 cm**. F**, Representative histological section showing peritoneal dissemination (asterisks) in $KP^{F/+}CS^{F/F}$ mice. Scale bars: 200 µm.

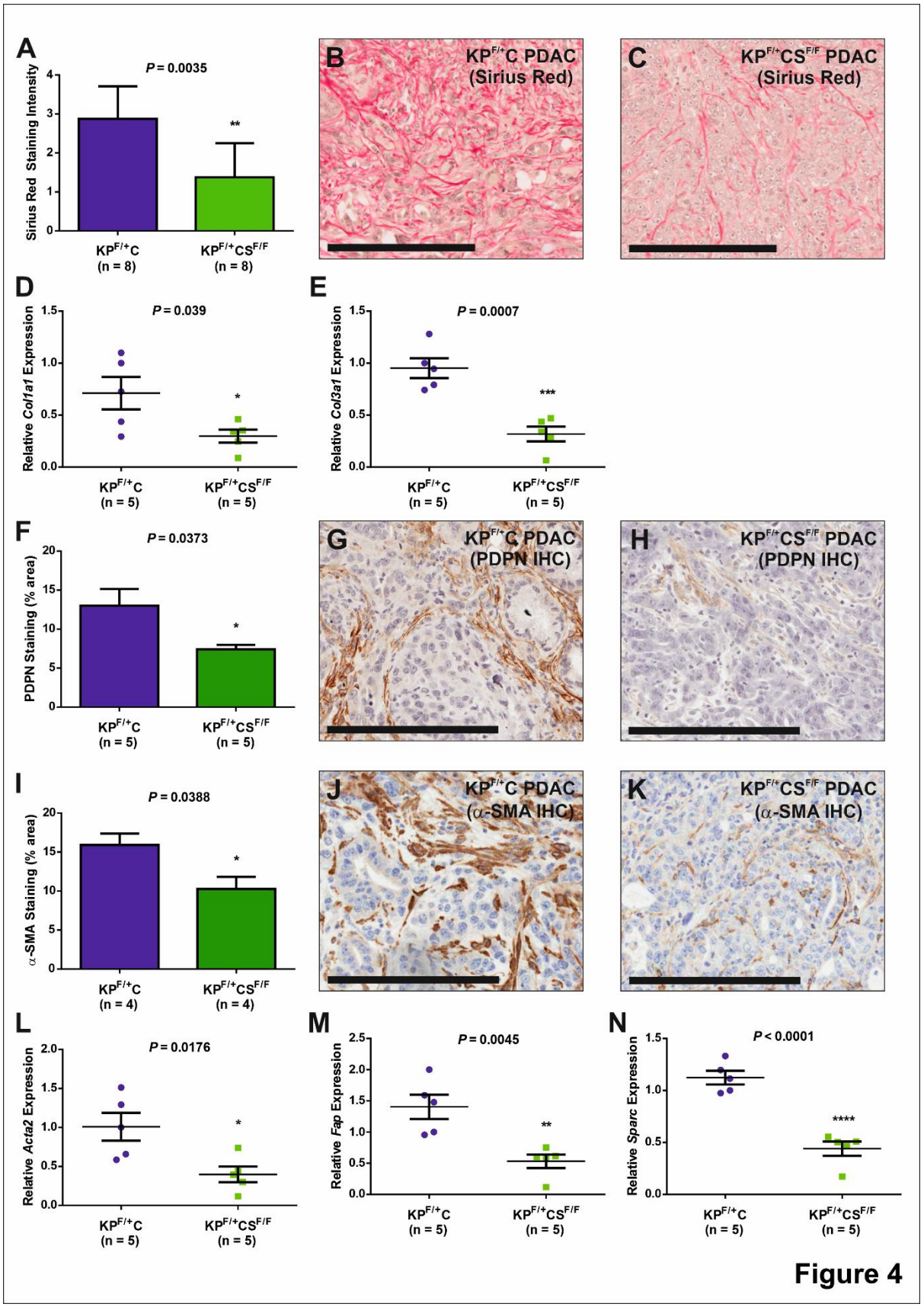
A
P = 0.0035
Sirius Red Staining Intensity
**
KP^F/+C (n = 8)
KP^F/+CS^F/F (n = 8)
B
KP^F/+C PDAC (Sirius Red)
C
KP^F/+CS^F/F PDAC (Sirius Red)
D
P = 0.039
Relative Col1a1 Expression
*
KP^F/+C (n = 5)
KP^F/+CS^F/F (n = 5)
E
P = 0.0007
Relative Col3a1 Expression
***
KP^F/+C (n = 5)
KP^F/+CS^F/F (n = 5)
F
P = 0.0373
PDPN Staining (% area)
*
KP^F/+C (n = 5)
KP^F/+CS^F/F (n = 5)
G
KP^F/+C PDAC (PDPN IHC)
H
KP^F/+CS^F/F PDAC (PDPN IHC)
I
P = 0.0388
α-SMA Staining (% area)
*
KP^F/+C (n = 4)
KP^F/+CS^F/F (n = 4)
J
KP^F/+C PDAC (α-SMA IHC)
K
KP^F/+CS^F/F PDAC (α-SMA IHC)
L
P = 0.0176
Relative Acta2 Expression
*
KP^F/+C (n = 5)
KP^F/+CS^F/F (n = 5)
M
P = 0.0045
Relative Fap Expression
**
KP^F/+C (n = 5)
KP^F/+CS^F/F (n = 5)
N
P < 0.0001
Relative Sparc Expression
****
KP^F/+C (n = 5)
KP^F/+CS^F/F (n = 5)

Figure 4

Figure 4. *Scrib*-null tumors exhibit reduced collagen and CAF contents. A, Column chart showing Sirius Red staining intensity in $KP^{F/+}C$ and $KP^{F/+}CS^{F/F}$ tumors. Results show the mean, s.e.m. and *P-values* (unpaired t-test). **B-C**, Representative histological section exhibiting Sirius Red staining in $KP^{F/+}C$ (**B**) and $KP^{F/+}CS^{F/F}$ (**C**) tumors. Scale bars: 200 µm. **D-E**, qPCR analysis of *Col1a1* (**D**) and *Col3a1* (**E**) in $KP^{F/+}C$ and $KP^{F/+}CS^{F/F}$ tumors. Results show the mean, s.e.m and *P-values* (unpaired t-test). **F**, Column chart showing PDPN staining (% area) in $KP^{F/+}C$ and $KP^{F/+}CS^{F/F}$ tumors. Results show the mean, s.e.m and P-values (unpaired t-test). **G-H**, Representative immunohistochemical staining of PDPN in $KP^{F/+}C$ (**G**) and $KP^{F/+}CS^{F/F}$ (**H**) tumors. Scale bars: 200 µm. **I**, Column chart showing α-SMA staining (% area) in $KP^{F/+}C$ and $KP^{F/+}CS^{F/F}$ tumors. Results show the mean, s.e.m. and *P-values* (unpaired t-test). **J-K**, Representative immunohistochemical staining of α-SMA in $KP^{F/+}C$ (**J**) and $KP^{F/+}CS^{F/F}$ (**K**) tumors. Scale bars: 200 µm. **L-N**, qPCR analysis of *Acta2* (**L**), *Fap* (**M**) and *Sparc* (**N**) in $KP^{F/+}C$ and $KP^{F/+}CS^{F/F}$ tumors. Results show the mean, s.e.m. and *P-values* (unpaired t-test).

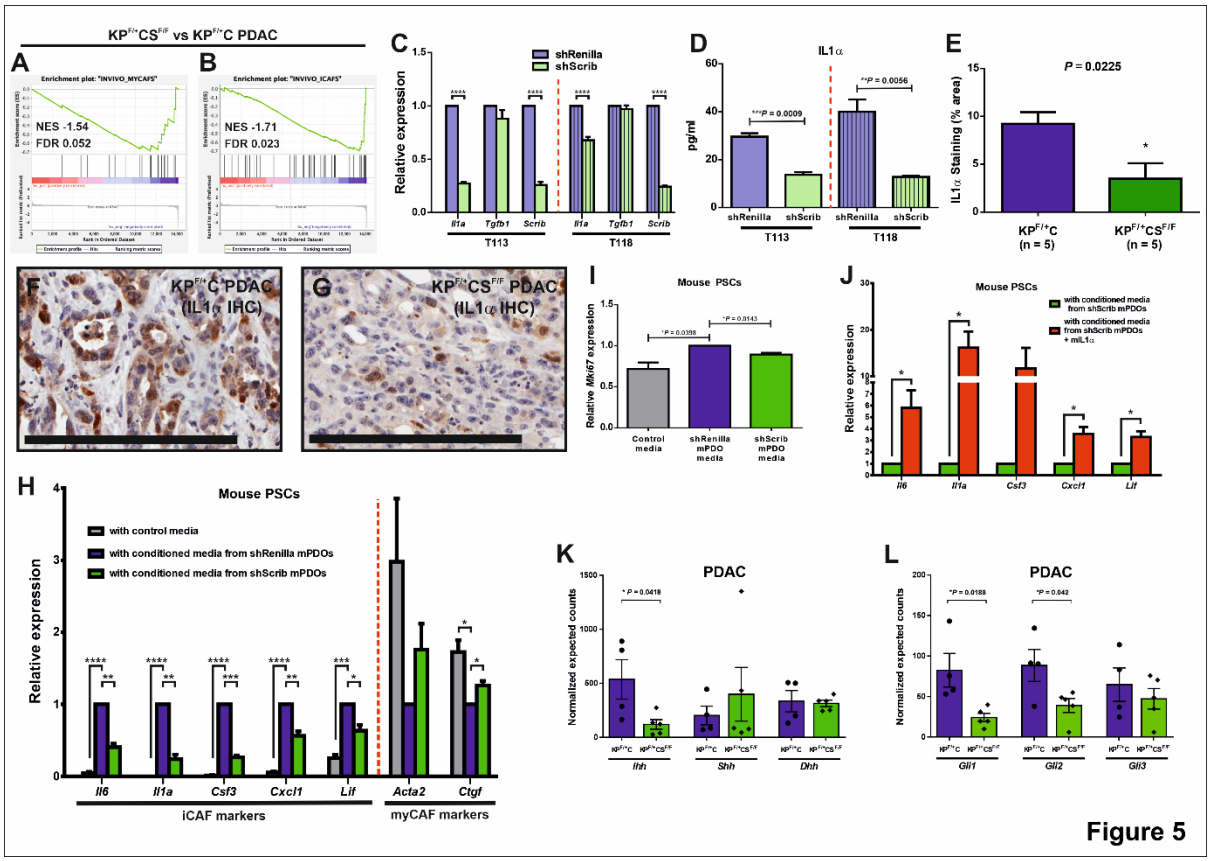

Figure 5. *Scrib* deficiency diminishes fibroblast activation. A-B, GSEA of myCAF (**A**) and iCAF (**B**) signatures in KP$^{F/+}$C (n = 4) and KP$^{F/+}$CS$^{F/F}$ (n = 5) tumors. NES, normalized enrichment score; FDR, false discovery rate. **C**, qPCR analysis of *Il1a*, *Tgfb1* and *Scrib* in shRenilla and shScrib mPDOs (T113 and T118) cultured in organoid media. Results show the mean and s.e.m. of 3 independent qPCRs (****P* < 0.001, *****P* < 0.0001; unpaired t-test). **D**, ELISA of IL1α from media of shRenilla and shScrib (T113 and T118) mPDOs (n = 3). Results show the mean and s.e.m and *P-values* (unpaired t-test). **E**, Column chart showing IL1α staining (% area) in KP$^{F/+}$C and KP$^{F/+}$CS$^{F/F}$ tumors. Results show the mean, s.e.m and *P*-values (unpaired t-test). **F-G**, Representative immunohistochemical staining of IL1α in KP$^{F/+}$C (**F**) and KP$^{F/+}$CS$^{F/F}$ (**G**) tumors. Scale bars: 200 µm. **H**, qPCR analysis of iCAF (*Il6*, *Il1a*, *Csf3*, *Cxcl1* and *Lif*) and myCAF (*Acta2* and *Ctgf*) markers in mouse PSCs cultured in Matrigel with control media or conditioned media from shRenilla and shScrib mPDOs for 4 days. Results show the mean and s.e.m. of 4 biological replicates (**P* < 0.05, ***P* < 0.01, ****P* < 0.001, *****P* < 0.0001; paired t-test). **I**, qPCR analysis of *Ki67* in mouse PSCs cultured in Matrigel with control media or conditioned media from shRenilla and shScrib mPDOs for 4 days. Results show the mean, s.e.m. and *P-values* (paired t-test) of 4 biological replicates. **J**, qPCR analysis of iCAF (*Il6*, *Il1a*, *Csf3*, *Cxcl1* and *Lif*) markers in mouse PSCs cultured in Matrigel with conditioned media from shScrib mPDOs in the presence or absence of 20 pg/ml IL1α for 4 days. Results show the mean and s.e.m. of 4 biological replicates (**P* < 0.05, paired t-test). **K-L**, Normalized expression of the Hedgehog ligands (*Ihh*, *Shh* and *Dhh*) (**K**) and Hedgehog transcriptional regulators (*Gli1*, *Gli2* and *Gli3*) (**L**) from bulk RNA-seq data of KP$^{F/+}$C (n = 4) and KP$^{F/+}$CS$^{F/F}$ (n = 5) PDAC tumors. Results show the mean, s.e.m. and P-values (unpaired t-test).

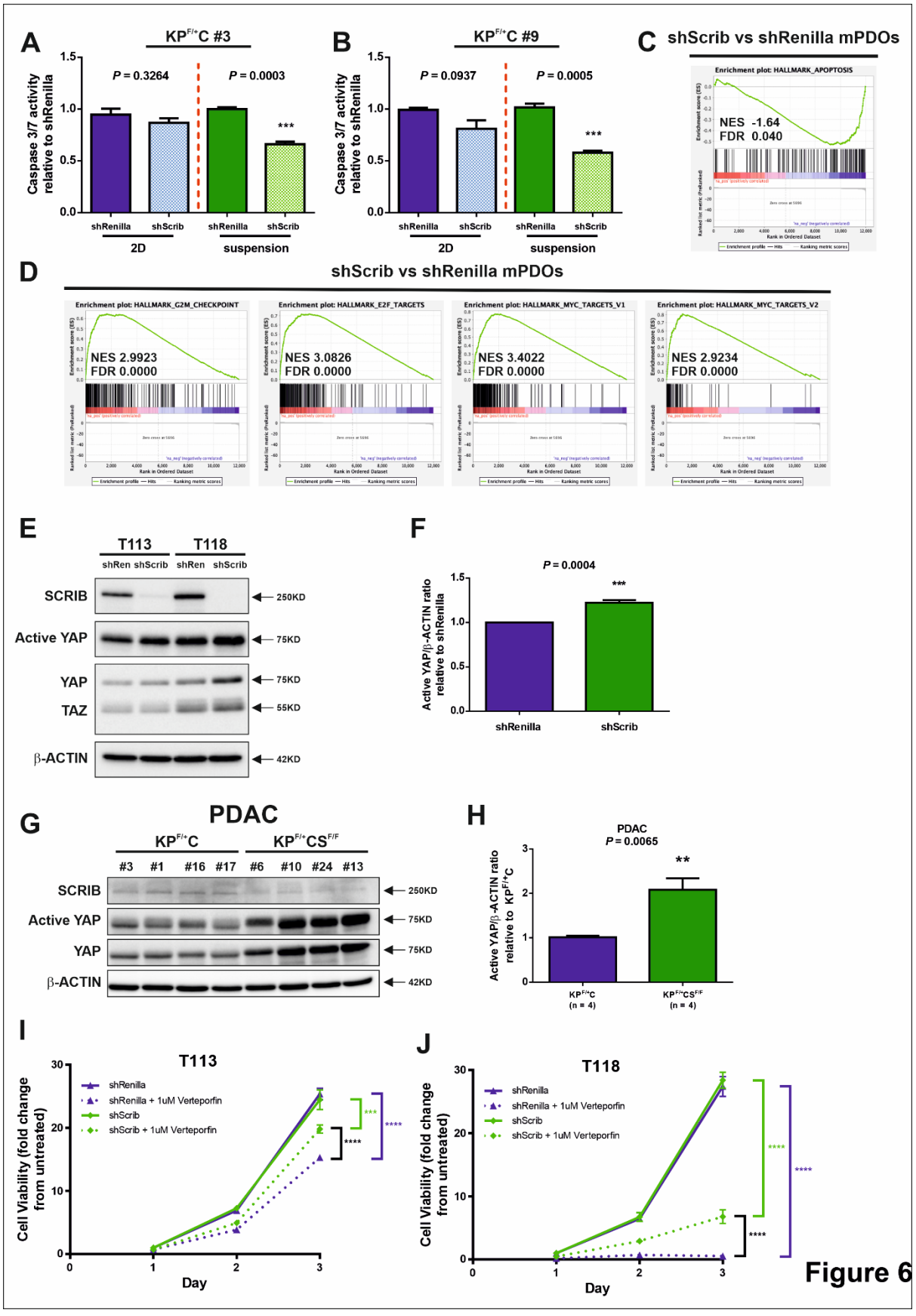
A
KP$^{F/+}$C #3
P = 0.3264
P = 0.0003
***
Caspase 3/7 activity relative to shRenilla
shRenilla
shScrib
shRenilla
shScrib
2D
suspension
B
KP$^{F/+}$C #9
P = 0.0937
P = 0.0005
***
Caspase 3/7 activity relative to shRenilla
shRenilla
shScrib
shRenilla
shScrib
2D
suspension
C
shScrib vs shRenilla mPDOs
Enrichment plot: HALLMARK_APOPTOSIS
NES -1.64
FDR 0.040
D
shScrib vs shRenilla mPDOs
Enrichment plot: HALLMARK_G2M_CHECKPOINT
NES 2.9923
FDR 0.0000
Enrichment plot: HALLMARK_E2F_TARGETS
NES 3.0826
FDR 0.0000
Enrichment plot: HALLMARK_MYC_TARGETS_V1
NES 3.4022
FDR 0.0000
Enrichment plot: HALLMARK_MYC_TARGETS_V2
NES 2.9234
FDR 0.0000
E
T113
T118
shRen shScrib shRen shScrib
SCRIB
250KD
Active YAP
75KD
YAP
75KD
TAZ
55KD
β-ACTIN
42KD
F
P = 0.0004
***
Active YAP/β-ACTIN ratio relative to shRenilla
shRenilla
shScrib
G
PDAC
KP$^{F/+}$C
KP$^{F/+}$CS$^{F/F}$
#3 #1 #16 #17 #6 #10 #24 #13
SCRIB
250KD
Active YAP
75KD
YAP
75KD
β-ACTIN
42KD
H
PDAC
P = 0.0065
**
Active YAP/β-ACTIN ratio relative to KP$^{F/+}$C
KP$^{F/+}$C (n = 4)
KP$^{F/+}$CS$^{F/F}$ (n = 4)
I
T113
shRenilla
shRenilla + 1uM Verteporfin
shScrib
shScrib + 1uM Verteporfin
***
****
****
Cell Viability (fold change from untreated)
Day
J
T118
shRenilla
shRenilla + 1uM Verteporfin
shScrib
shScrib + 1uM Verteporfin
****
****
****
Cell Viability (fold change from untreated)
Day

Figure 6

Figure 6. *Scrib* downregulation increases cell survival and YAP activation in mouse PDAC cells. **A-B**, Caspase-3/7 activity in KPC#3 (**A**) and KPC#9 (**B**) cells grown in suspension or 2-dimensional cultures for 48 hours. Results show the mean, s.e.m. and *P-values* (unpaired t-test) of 3 biological replicates. **C-D**, GSEA of the apoptosis (**C**) and cell cycle progression related (G2M checkpoint, E2F targets and MYC targets) (**D**) gene signatures in shScrib versus shRenilla mPDOs (n = 3). NES, normalized enrichment score; FDR, false discovery rate. **E**, Western blot analysis showing active YAP, total YAP and TAZ protein levels in shRenilla and shScrib mPDOs (T113 and T118). β-ACTIN is used as loading control. **F**, Quantification of active YAP levels in shScrib mPDOs relative to shRenilla mPDOs (n = 4). Results show the mean, s.e.m. and P-values (unpaired t-test). **G**, Western blot analysis showing active YAP and total YAP protein expression in $KP^{F/+}C$ and $KP^{F/+}CS^{F/F}$ PDAC tumors. β-ACTIN is used as loading control. **H**, Quantification of active YAP levels in $KP^{F/+}CS^{F/F}$ PDAC relative to $KP^{F/+}C$ PDAC. Results show the mean, s.e.m. and *P-values* (unpaired t-test). **I-J**, Proliferation curves of shRenilla and shScrib T113 (**I**) and T118 (**J**) mPDOs cultured in the presence or absence of 1 μM Verteporfin. Results show the mean and s.d. of 5 technical replicates (***$P < 0.001$; ****$P < 0.0001$; unpaired t-test calculated for the last time point). The experiment was performed twice with similar result.

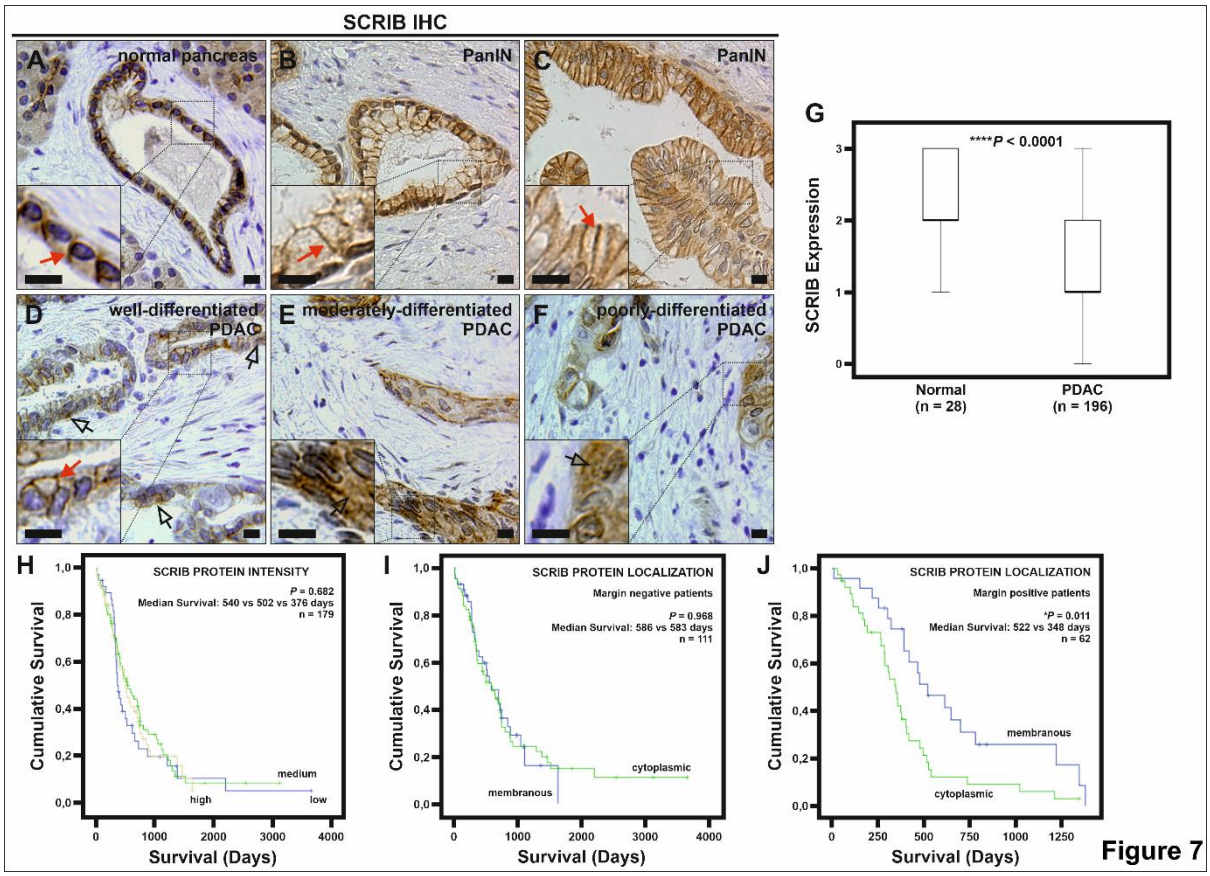

Figure 7. SCRIB expression is altered in human PDAC. A-F, Representative immunohistochemical staining of membranous SCRIB (red arrow) in normal pancreas ducts (**A**) and PanIN lesions (**B**, **C**), membranous (red arrow) and cytoplasmic (open arrow) SCRIB in well-differentiated PDAC (**D**), and cytoplasmic (open arrow) SCRIB in moderately-differentiated (**E**) and poorly-differentiated (**F**) PDAC. Scale bars: 5 μm. **G**, Boxplot comparing SCRIB protein expression by immunohistochemical detection in PDAC (n = 196; median = 1) and adjacent normal tissue (n = 28; median = 2) (P < 0.0001; Chi-Square test). **H**, Kaplan-Meier survival curve of individuals with resected PDAC (n = 179) that express low (376 days, blue line, n = 39), medium (540 days, green line, n = 81) or high (502 days, yellow line, n = 59) levels of SCRIB protein (*P* = 0.682; log-rank test). **I**, Kaplan-Meier survival curve of individuals with negative surgical margin (n = 111) that express only membranous (586 days, blue line, n = 43) versus some or all cytoplasmic (583 days, green line, n = 68) SCRIB protein (*P* = 0.968; log-rank test). **J**, Kaplan-Meier survival curve of individuals with positive surgical margin (n = 62) that express only membranous (522 days, blue line, n = 24) versus some or all cytoplasmic (348 days, green line, n = 38) SCRIB protein (*P* = 0.011; log-rank test).

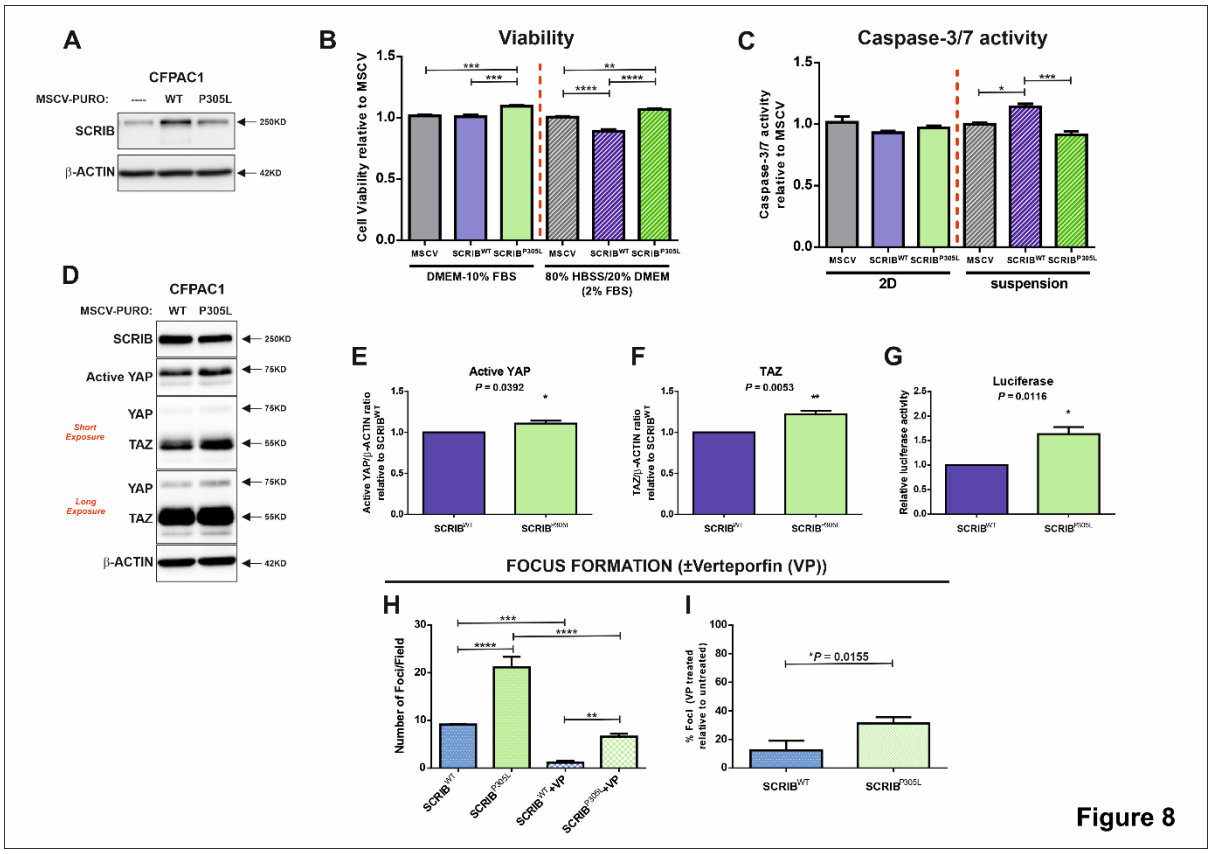

Figure 8. Cytoplasmic SCRIB^{P305L} does not retain tumor suppressor properties in PDAC cells. **A**, Western blot analysis showing SCRIB^{WT} (WT) and SCRIB^{P305L} (P305L) protein expression, compared to CFPAC1 cells transduced with MSCV-PURO empty vector (----). β-ACTIN is used as loading control. **B**, Cell viability of CFPAC1 cells transduced with MSCV-PURO (MSCV), MSCV-PURO-hSCRIB^{WT} (SCRIB^{WT}) and MSCV-PURO-hSCRIB^{P305L} (SCRIB^{P305L}) and cultured in DMEM-10% FBS or 80% HBSS/20% DMEM (2%FBS) media for 3 days. Results show the, s.d. and *P-values* (***P* < 0.01, ****P* < 0.001, *****P* < 0.0001; One-way ANOVA with Bonferroni post-test) of 5 technical replicates. The experiments were performed twice with similar result. **C**, Caspase-3/7 activity of CFPAC1 cells transduced with MSCV-PURO, MSCV-PURO-hSCRIB^{WT} and MSCV-PURO-hSCRIB^{P305L} grown in suspension or 2-dimensional cultures for 48 hours. Results show the mean, s.e.m. and *P-values* (**P* < 0.05, ****P* < 0.001; One-way ANOVA with Bonferroni post-test) of 3 biological replicates. **D**, Western blot analysis showing active YAP, total YAP and TAZ protein expression in CFPAC1 cells ectopically expressing SCRIB^{WT} (WT) or SCRIB^{P305L} (P305L). β-ACTIN is used as loading control. **E-F**, Quantification of active YAP (**E**) and TAZ (**F**) levels in CFPAC1-SCRIB^{P305L} (SCRIB^{P305L}) cells relative to CFPAC1-SCRIB^{WT} (SCRIB^{WT}) cells (n = 3). Results show the mean, s.e.m. and *P-values* (unpaired t-test). **G**, Quantification of YAP/TAZ-responsive reporter (8xGTIIC-Luc) activity in CFPAC1-SCRIB^{WT} and CFPAC1-SCRIB^{P305L} cells. Results show the mean, s.e.m. and *P-value* (unpaired t-test) of 3 biological replicates. **H**, Column chart showing foci quantification of CFPAC1-SCRIB^{WT} and CFPAC1-SCRIB^{P305L} cells cultured in the presence or absence of 4 μM Verteporfin (VP). Results show the mean, s.e.m. and *P-values* (***P* < 0.01, ****P* < 0.001, *****P* < 0.0001; One-way ANOVA with Bonferroni post-test) of 3 biological replicates. **I**, Column chart showing the % foci formed by CFPAC1-SCRIB^{WT} and CFPAC1-SCRIB^{P305L} cells cultured in the presence of 4 μM Verteporfin (VP) relative to CFPAC1-SCRIB^{WT} and CFPAC1-SCRIB^{P305L} cells cultured in the absence of VP. Results show the mean, s.e.m. and *P-value* (unpaired t-test) of 3 biological replicates.